AMERICAN UNIVERSITY OF BEIRUT

ON THE LINEAR AND NONLINEAR DYNAMICS OF THE HASEGAWA-MIMA EQUATION

by
AKASHA SHADI KABBOUL

A thesis
submitted in partial fulfillment of the requirements
for the degree of Master of Science
to the Department of Physics
of the Faculty of Arts and Sciences
at the American University of Beirut

Beirut, Lebanon
February 2025

AMERICAN UNIVERSITY OF BEIRUT

ON THE LINEAR AND NONLINEAR DYNAMICS OF THE HASEGAWA-MIMA EQUATION

by

AKASHA SHADI KABBOUL

Approved by:

Dr. Ghassan Antar, Professor — Advisor

Department of Physics

Dr. Sophie Moufawad, Assistant Professor — Member of Committee

Department of Mathematics

Dr. Sadruddin Benkadda, Professor — Member of Committee

Department of Physics, Aix-Marseille University, France

Date of thesis defense: February 26, 2025

Acknowledgements

I would like to extend my sincere gratitude to Dr. Antar for his guidance throughout this journey and for the many insightful, thought-provoking discussions that made working on this thesis truly enjoyable.

I would also like to thank Dr. Moufawad for her invaluable help in navigating the simulations and Dr. Benkadda for taking the time to engage with this work.

To my family, who have provided me with unwavering support and love that have been my anchor through it all.

And to my solace, Ayman, whose support has meant more than words can express.

I am endlessly grateful.

Abstract
of the Thesis of

Akasha Shadi Kabboul for Master of Science
Major: Physics

Title: On the Linear and Nonlinear Dynamics of the Hasegawa-Mima Equation

Understanding turbulence in plasmas is essential for studying transport properties in magnetically confined fusion devices. This thesis studies the Hasegawa-Mima (HM) model, which describes the evolution of electrostatic potential fluctuations in a plasma. First, we derive the HM model from first principles using fundamental conservation equations.

Analytical studies of the HM model are then performed to investigate the role of the linear term and its effect on the system dynamics. In particular, this study explores the evolution of an initial electrostatic potential perturbation initialized as white noise. The effect of the linear term on the dynamics is highlighted through its dependence on the density gradient. The steepness of the density profile is varied, therefore, assessing the impact of the linear term on the overall dynamics.

Then, numerical simulations of the HM model are conducted using FreeFEM++. The simulation results are then analyzed in light of the analytical results. The results show that an increase in the amplitude of the electrostatic potential occurs in the gradient region, and there is no spreading of the turbulence beyond that region.

Table of Contents

Illustrations

Tables

Chapter 1

Introduction

1.1 Motivation

Every realistic system possesses an inherent background white noise, and this is namely the case for fusion plasmas as well as for other phenomena. In this thesis, the goal is to understand the evolution of white noise and how turbulence spreads according to the Hasegawa-Mima equation. This study is first done analytically, using simplified cases that simulate white noise initial conditions. The results are then compared to the simulation results of the Hasegawa-Mima equation. The simulation is conducted using the finite element method code written in FreeFem++ [1] to simulate the evolution, and the gradient of the density profile is varied while maintaining the initial potential field as white noise.

1.2 Plasma

Plasma is an ionized gas. A plasma forms when a solid is heated enough that the thermal motion of the atoms breaks the crystal lattice structure apart, which forms a liquid. Then, the liquid is heated sufficiently that atoms vaporize off the surface faster than they recondense, which forms a gas. Then, in turn, the gas is heated enough that the atoms collide and knock their electrons off, and thus a plasma is formed. Plasma is also referred to as the 'fourth state of matter.' In a plasma, charge separation between ions and electrons creates electric fields, and the motion of charged particles creates currents and magnetic fields [2].

The most fundamental plasma property is its quasi-neutrality. This is because the densities of electrons n_e and ions n_i in plasma are almost equal. This is due to the large charge-to-mass ratio of electrons, so any significant imbalance of charge creates an electric field strong enough to drag a neutralizing cloud of electrons into the positively charged region. So, because of the electron inertia, they oscillate

about the initially charged region at high frequency and thus maintain quasi-neutrality [3]. This phenomenon is known as *Debye Shielding*. A helpful parameter to define in this case is the Debye length λ_D, which is the value below which quasi-neutrality ceases and above which it is maintained; therefore, the Debye length is a measure of the shielding distance. In addition, it is a criterion for an ionized gas to be plasma, such that if the dimensions of the system are much larger than λ_D, then it is plasma. To define an expression of λ_D, it must first be noted that it increases as kT_e increases, where k is the Boltzmann constant. So the electron temperature must be used in defining λ_D since electrons are more mobile than ions and do the shielding themselves[4]. Thus, the Debye length is defined as

$$\lambda_D = \sqrt{\frac{\epsilon_0 k_B T_e}{n_e q^2}}, \tag{1.1}$$

Where ϵ_0 is the permittivity of free space, k_B is the Boltzmann constant, T_e is the electron temperature, n_e is the electron density, and q is the charge of the electron.

1.3 Plasma in Nature

In nature, plasma is abundant and can be found in various environments, ranging from the interiors of stars to the Earth's atmosphere. One example of that is stars, which are massive celestial bodies primarily composed of plasma [5]. The extreme temperatures and pressures in a star's core cause hydrogen atoms to undergo nuclear fusion, forming helium and releasing an enormous amount of energy. This process generates a high-temperature plasma state within the stars. Additionally, another example is the solar wind, which is a stream of charged particles the sun continuously releases. The light during the daytime results from the plasma present in the sun's photosphere, and moonlight is essentially a reflection of that sunlight. During the night, the visible light from stars and nebulas originates from their plasma [6]. Therefore, the absence of plasma would lead to significant darkness in the absence of these sources of light. Aurora borealis, also known as Northern Lights, and aurora australis, or Southern Lights, are phenomena caused by the interaction of charged particles from the solar wind with the Earth's magnetosphere [7]. The excited gases in the Earth's upper atmosphere emit light, creating colorful displays. The ionization of gases in the atmosphere during this process results in the formation of plasma. Lightning is another natural phenomenon that involves plasma. During a thunderstorm, the buildup of electrical potential between the ground and the atmosphere leads to the discharge of electricity in the form of a lightning bolt. This discharge ionizes the air along its path, creating a temporary plasma channel.

1.4 Plasma Applications

The other type of plasma is man-made plasma, which has numerous applications in different fields, one of which is plasma used in fusion energy research, which we've already mentioned. A prominent use of plasma is in lighting, where some types of energy-efficient lighting use plasma to produce visible light, such as fluorescent lights and neon signs. These devices rely on the ionization of gases to emit light [8]. Plasma has also proven useful in the medical domain for sterilization purposes. Cold plasma can be applied to disinfect surfaces and medical instruments without causing damage or raising temperatures significantly. Industrially, partially ionized plasmas with high density find various applications. Magnetrons are employed in sputtering, a technique for coating materials. Plasmas are utilized to coat eyeglasses, generate arcs for searchlights, and thoroughly clean instruments in medical research [4].

Another application of plasma is semiconductor manufacturing. Plasma is employed in the semiconductor industry for processes such as plasma etching and plasma deposition. Plasma etching removes material from semiconductor wafers with high precision, while plasma deposition helps deposit thin films on the wafer surfaces for various purposes, including creating electronic components.

Plasmas are typically generated in vacuum systems, but it is also possible to create them at atmospheric pressure. One method involves ionizing a jet of argon and helium using radio-frequency power. This allows the development of small, compact devices, like small pencils, for skin cauterization. Industrial substrates can be treated by sweeping such a jet to cover extensive areas.

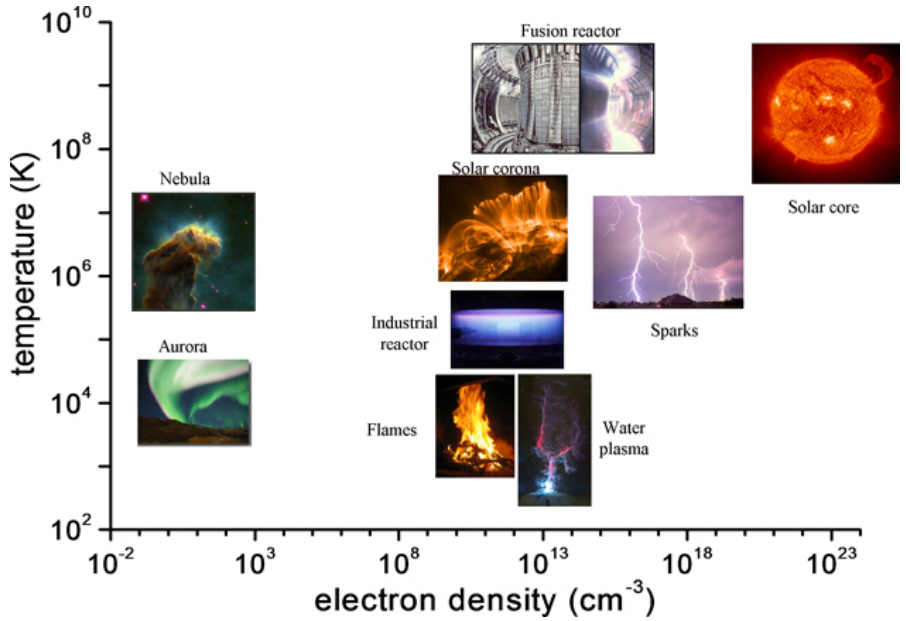

Figure 1.1: Types of plasma

1.5 Thermonuclear Fusion Plasma

The sun brings huge amounts of energy to the planetary system in the form of solar light produced by massive fusion reactions. A large number of scientists in the latter half of the twentieth century strove to create energies of that scale on Earth using fusion.

In a fusion reaction, two light nuclei merge to form a heavier nucleus. The process releases energy because the total mass of the resulting single nucleus is less than the mass of the two original nuclei (according to the fundamental equation $E = mc^2$). Fusion requires deuterium and tritium nuclei, two isotopes of hydrogen, as fuel, and these two elements happen to be very abundant in nature, as deuterium exists naturally as one part in 6000 of water.

Thermonuclear fusion occurs when the fuel is heated sufficiently so that the thermal velocities of the particles are large enough to produce the required fusion reactions. To start fusion, the nuclei should be maintained close together at a very high temperature for a very short time [9]. However, this step is the most difficult since it needs a large number of nuclei to increase the probability of collision, and the particles should remain confined for a sufficient period of time leading to fusion.

One of the most promising magnetic fusion configuration, 'tokamak,' was initiated in the Soviet Union [10]. The word 'tokamak' [11] is an acronym from the Russian word for toroidal chamber with an axial magnetic field. It is used in nuclear fusion research for the magnetic confinement of plasma and consists of a system of magnetic fields that confine the plasma in a hollow, doughnut-shaped container.

Magnetic confinement takes advantage of the charge of plasma particles and attempts to design a magnetic field to confine plasma for a long time. In a fusion reactor and at very high temperatures, the isotopes of hydrogen gas form a state known as the plasma state, which is an ionized gas where atoms of the gas have lost one or more of their electrons. Once we apply a magnetic field, plasma particles rotate around field lines in a helical motion.

The traditional deuterium-tritium (DT) fusion reaction is given by [12]:

$$\mathrm{D} + \mathrm{T} \rightarrow^{4} \mathrm{He}(3.52\mathrm{MeV}) + \mathrm{n}(14.07\mathrm{MeV}) \tag{1.2}$$

One essential area of study aims to understand how a thermonuclear plasma can be trapped by a magnetic field and investigate the different types of plasma instabilities that could occur and cause it to escape the confinement. One type of confinement used is the inertial confinement which is the process of creating

high-temperature, high-density plasma by compressing and heating a small target, typically a pellet consisting of an outer layer of radiation absorbing material, and an inner layer of deuterium and tritium fuel [13]. This pellet is hit by powerful laser pulses. This eventually creates a central hot spot, where the fusion reactions begin. If conditions are right, the heat from these reactions ignites the surrounding fuel, leading to a self-sustained burn wave, releasing energy [14]. For our purposes, we will be focusing on magnetic confinement fusion which will be discussed further in the next section.

1.6 Magnetic Confinement Devices

1.6.1 *Tokamaks*

Approaching fusion from a more experimental perspective shows that to induce the fusion of nuclei of deuterium and tritium, the mutual repulsion due to their positive charges must first be overcome. This repulsion results in the cross-section for fusion being small at low energies; however, the cross-section increases with energy, reaching a maximum at 100 keV, and a positive energy balance is possible if the reaction of fuel particles can be induced before they lose their energy. So, this requires the particles to retain their energy and remain in the region where they can react for enough time. To state those conditions mathematically, the product of this time and the density of reacting particles should be large enough.

The most suitable method of satisfying these conditions is to heat the deuterium-tritium fuel to a temperature high enough that the thermal velocities of the nuclei are sufficiently high to produce the fusion reactions, and this method of achieving fusion is referred to as thermonuclear fusion [15].

Tokamaks consist of toroidal (doughnut-shaped) and poloidal (vertical) coils. This is because a toroidal configuration alone cannot sustain fusion since there exists a particle drift up or down caused by the magnetic field curvature. Therefore, to counteract this motion, poloidal coils are introduced.

Prominent examples of tokamaks include the Joint European Torus (JET) in the United Kingdom, the Tokamak Fusion Test Reactor (TFTR) in the United States, and the International Thermonuclear Experimental Reactor (ITER), an international collaboration located in France. However, it is worth noting that in a setting such as the tokamak, plasma may become easily turbulent and unstable. Instabilities are regions where small perturbations grow rapidly. When plasma is at equilibrium, certain regions of it can be disturbed by small perturbations. The stability of the system determines if the perturbations will grow, oscillate, or be damped out. Therefore, numerous efforts have been devised for the development of mathematical models describing plasma during its confinement to better understand the evolution of turbulence and instabilities.

1.6.2 *Stellarators*

Another major device used for the magnetic confinement of plasma is the stellarator [16]. The concept of stellarators dates back to the mid-20th century when physicists began exploring alternative approaches to magnetic confinement for controlled nuclear fusion.

A stellarator is a toroidal plasma confinement device that uses effects caused by the absence of toroidal symmetry to maintain the magnetic configuration without the need for a current drive to maintain stability [17]. The key design feature of a stellarator is its carefully engineered magnetic coils, which produce a three-dimensional magnetic field. This unique field configuration eliminates the need for a plasma current, providing inherent stability and preventing disruptions.

Stellarators inherently possess stability against certain plasma instabilities. The twisted magnetic field minimizes the effect of turbulent plasma instabilities, leading to prolonged confinement times. They are also capable of continuous operation, making them suitable for steady-state plasma experiments. This is in contrast to tokamaks, which operate in short bursts.

Stellarators have significantly contributed to our understanding of plasma physics and fusion research. For instance, the experimental data obtained from stellarators serves as a crucial benchmark for validating and refining theoretical models related to plasma behavior, stability, and confinement. Stellarators also provide a platform for testing materials under extreme conditions, allowing scientists to evaluate the durability of components exposed to high-energy plasmas.

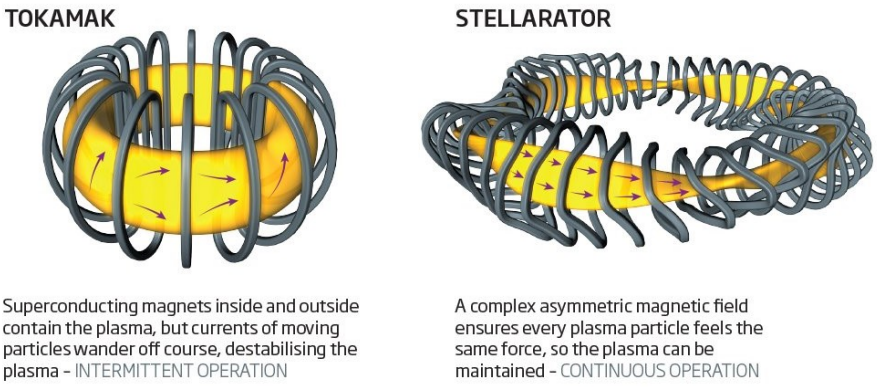

Figure 1.2: Tokamak versus Stellarator.

1.7 Turbulence

Turbulence is a complex and ubiquitous phenomenon observed in a wide range of systems, including fluids and plasma [18]. It represents a state of disorder

characterized by the irregular and chaotic motion of fluid elements -in the case of fluid- or charged particles -in the case of plasma- resulting in a seemingly random and fluctuating flow field. Understanding turbulence is of utmost importance as it plays a crucial role in shaping the behavior of plasma in various settings, and it especially plays a determining role when constructing a magnetic confinement system to perform fusion. Namely, drift wave turbulence is the main reason why the radial diffusion in tokamak magnetic plasma confinement devices is much worse than can be explained by simple random walks due to particle collisions [19].

When describing fluids, turbulence is encountered in everyday occurrences, from the flow of rivers and oceans to the motion of air in the atmosphere. The study of fluid turbulence has a rich history and has yielded valuable insights into the underlying dynamics of these systems however, when it comes to plasma, that becomes even more challenging due to the additional complexities introduced by magnetic fields, electric fields, and the inherently non-linear nature of plasma interactions.

The transition from laminar smooth flows to turbulent behavior in plasma can occur under different conditions, including high temperatures and magnetic confinement. Turbulence in plasma can manifest as fluctuations in temperature, density, and magnetic fields, impacting the overall stability and confinement of the plasma. Understanding these turbulent processes is critical for advancing the development of fusion energy.

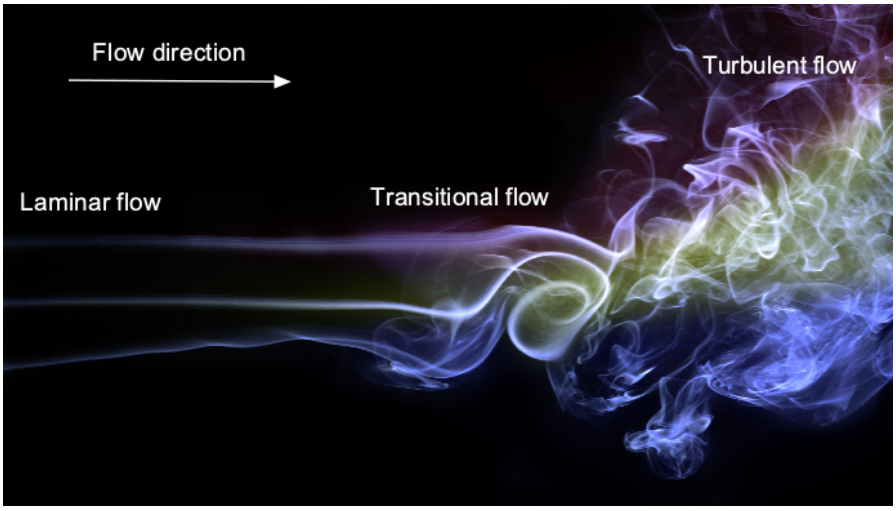

Figure 1.3: Transition from laminar flow to turbulence

1.8 The Role of Turbulence and Radial Transport in Confinement

In magnetic confinement devices such as tokamaks, stellarators' turbulent processes can disrupt the balance required for sustaining fusion reactions. Plasma turbulence leads to increased energy and particle losses, rendering the fusion reaction unviable. Therefore, to curb that effect, understanding the origins and dynamics of turbulence is essential.

Plasma turbulence can also lead to enhanced radial transport and reduced confinement times. Radial transport is the movement of particles and energy across the radial direction of the plasma and is closely connected to turbulence.

In 1957, J.D Lawson was one of the first people to examine the feasibility of controlled thermonuclear reactors, and he discovered criteria that must be met to make a thermonuclear reactor possible [20]. His criterion considers a perfectly general model, not associated with any particular method of confinement, and specifies the restrictions on parameters that would be placed on a fusion-reacting system to make it yield net power.

The Lawson criterion states that generating substantial amounts of fusion energy requires confining ample quantities of plasma fuel for an extended period. This means that the product $n\tau_e$ of the number density of fusing nuclei n and the time scale of confinement τ_e must be large. The energy confinement time is defined as $\tau_e = \frac{W}{P}$, where W is the energy content of the plasma and P is the rate of energy loss. Plasma reaches ignition when all energy losses are balanced by alpha particle heating and when no additional energy inputs are needed to maintain the fusion reaction.

1.9 Waves in Plasma

1.9.1 *Electron Plasma Waves*

The displacement of electrons in plasma from a uniform background of ions generates an electric field in a direction that restores the neutrality of the plasma. Because of their inertia, the electrons will overshoot and oscillate around their equilibrium positions with a frequency known as the plasma frequency [4]. Another cause of plasma oscillation propagation is thermal motion. Electrons flowing into adjacent layers of plasma carry information about what is happening in the oscillating region through their thermal velocities. This generates a plasma wave. To express these waves mathematically, we must first consider the electron momentum balance equation, which will be discussed in detail in Chapter 3.

$$n_e m_e [\frac{\partial \vec{u}_e}{\partial t} + (\vec{u}_e \cdot \vec{\nabla})\vec{u}_e] = -n_e e(\vec{E}) \tag{1.3}$$

Where:

n_e is the electron density,
m_e is the electron mass,
$\vec{u}_e$ is the electron velocity, and $\vec{u}_i$ is the ion velocity,
e is the electron charge,
$\vec{E}$ is the electric field,
$\vec{B}$ is the magnetic field,
$\vec{\nabla} p_e$ is the pressure gradient for electrons.

To account for the thermal motion, we add a pressure gradient term such that

$$n_e m_e [\frac{\partial \vec{u}_e}{\partial t} + (\vec{u}_e \cdot \vec{\nabla})\vec{u}_e] = -n_e e(\vec{E}) - \vec{\nabla} p_e \tag{1.4}$$

But according to the ideal gas law, the pressure gradient can be expressed as $\vec{\nabla} p_e = 3kT_e \vec{\nabla} n_e$. Following a perturbative approach, the density n_e can be expressed as $n_0 + n_1$ where n_0 is the initial density, and n_1 is the first order perturbation to the density. As such, we obtain $\vec{\nabla} p_e = 3kT_e \vec{\nabla}(n_0 + n_1) = 3kT_e(\partial n_1/\partial x)\hat{x}$ So, the momentum balance equation becomes

$$mn_0 \frac{\partial v_1}{\partial t} = -en_0 E_1 - 3kT_e \frac{\partial n_1}{\partial x} \quad \Rightarrow \quad im\omega n_0 v_1 = -en_0 E_1 - 3kT_e ik \frac{\partial n_1}{\partial x} \tag{1.5}$$

Expressing E_1 and n_1 in Fourier modes

$$\begin{aligned} im\omega n_0 v_1 &= \left[en_0 \left(-eik_0\right) + 3kT_e ik\right] n_0 i\omega v_1 \\ &\Rightarrow \omega^2 v_1 = \frac{n_0 e_0^2}{m} + \frac{3kT_e}{mk^2} v_1 \\ &\Rightarrow \omega^2 = \omega_p^2 + \frac{3}{2}\frac{k^2}{v_{th}^2} \end{aligned} \tag{1.6}$$

where $v_{th}^2 = 2kT_e/m$

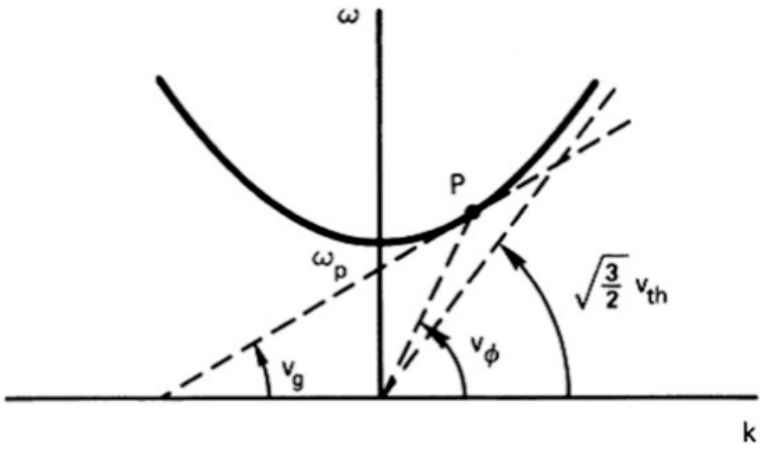

Figure 1.4: Dispersion Relation of Electron Waves in Plasma, adapted from [4]

1.9.2 *Sound Waves*

Due to the pressure gradient, sound waves are generated in plasma, whose dispersion relation we can obtain starting from the MHD momentum balance equation.

$$\rho\left[\frac{\partial\vec{v}}{\partial t}+(\vec{v}\cdot\vec{\nabla}\vec{v})\right]=-\vec{\nabla}p=-\frac{\gamma p}{\rho}\vec{\nabla}\rho \tag{1.7}$$

where ρ is the mass density defined as $\rho = n_i m_i + n_e m_e \approx n(m_i + m_e)$

$$\frac{\partial\rho}{\partial t}+\vec{\nabla}\cdot(\rho\vec{v})=0 \tag{1.8}$$

Linearizing about a stationary equilibrium with uniform p_0 and ρ_0

$$\begin{aligned} -i\omega\rho_0 v_1 &= -\frac{\gamma p_0}{\rho_0} ik\rho_1 \\ -i\omega\rho_1 + \rho_0 i\vec{k}\cdot\vec{v}_1 &= 0 \end{aligned} \tag{1.9}$$

For a plane wave with $\vec{k} = k\hat{x}$ and $\vec{v} = v\hat{x}$; eliminating ρ_1

$$\begin{aligned} -i\omega\rho_0 v_1 &= -\frac{\gamma p_0}{\rho_0} ik \frac{\rho_0 ikv_1}{i\omega} \\ \omega^2 v_1 &= k^2\frac{\gamma p_0}{\rho_0} v_1 \\ \frac{\omega}{k} &= \left(\frac{\gamma p_0}{\rho_0}\right)^{1/2} = \left(\frac{\gamma kT}{M}\right)^{1/2} \equiv c_s \end{aligned} \tag{1.10}$$

c_s is the speed of sound waves in a neutral gas. The dispersion relation obtained is that of pressure waves propagating from one layer to another through collisions among the air molecules.

1.10 Thesis Outline

In chapter 2, a literature review of selected relevant works on the Hasegawa-Mima and Hasegawa-Wakatani models will be discussed. In chapter 3, the HM and HW models will be derived starting from basic assumptions and the momentum balance and continuity equations. Chapter 4 will cover analytical methods in studying the HM model, leading to a simplified estimate of white noise as an initial electrostatic potential. Additionally, chapter 5 will cover the analytical study of the HW model, deriving the effective Reynolds number and the dispersion relation of the HW model. Finally, in chapter 6, the simulation results will be presented along with the corresponding statistical analysis.

Chapter 2

Literature Review

2.1 Literature on the Hasegawa-Mima Model

The Hasegawa-Mima model was first derived in Ref. [21], where Hasegawa and Mima derived an equation to describe turbulence in a nonuniform plasma where the temporal time scale is much larger than the ion cyclotron period. The paper assumed that the electron temperature is much larger than the ion temperature. If the parallel-phase velocity is smaller than the electron thermal speed, the parallel motion of electrons becomes important.

The equation derived is then used to explain the spectrum of density fluctuations observed in the ATC Tokamak. This paper aims to identify the important nonlinear term and the derivation of a simple nonlinear equation appropriate to a general class of quasi-two-dimensional low-frequency turbulence. The other is the solution of the equation using the renormalized-weak-turbulence technique and comparison of the result with the experimental data. The equation derived then indicates that pseudo-three-dimensional plasma behaves like an incompressible fluid for a short perpendicular wavelength, but for a long perpendicular wavelength, the compressibility correction becomes important, and the nonlinear term of our equation is identical to that of the Navier-Stokes equation if the electrostatic potential is replaced by the z-component of the vector potential for the velocity field.

The result of the simulation based on the Hasegawa-Mima model presents an ω integrated k spectral density that shows an overlap with the experimental results for long wavelength but a discrepancy in the short wavelength due to the finite ion gyroradius effect and the ion Landau damping which the model does not account for. The HM model was first used to interpret density fluctuation spectra observed in the ATC Tokamak.

2.1.1 *Other Related Models*

One notable model is the Charney-Hasegawa-Mima (CHM) equation, which emerges from the mathematical isomorphism between the HM equation, used to describe drift waves in plasmas, and the Charney equation, originally introduced in Ref. [22] to describe Rossby waves in geophysical fluid dynamics. While these equations were independently developed in plasma and atmospheric physics, their formal similarity has led to a unified mathematical treatment, often referred to as the CHM equation.

Ref. [23] discusses the CHM model by combining the HM equation and the Rossby wave equation. The article explores both the statistical properties of this model, analyzing its spectra, and its coherent structures, deriving from vortex solutions. Furthermore, a stability analysis is performed to examine the stability of vortices arising from the self-organization of turbulent structures.

Another relevant model is the Hasegawa-Wakatani model, which is discussed at length in B.

2.1.2 *Numerical Studies on the Hasegawa-Mima Model*

More recent papers have focused on studying the HM model through simulations and numerical approaches. In Ref. [24], the evolution of decaying turbulence was studied by solving the HM equation. It was also concluded that the system evolves naturally to a quasi-steady state characterized by large coherent monopole vortices and a narrow frequency spectrum.

In Ref. [25], Botha emphasized the effect of the density n_0 profile on the generation of a sheared diamagnetic flow and how that affects turbulence.

Ref. [26] conducted a numerical study of the Generalized Charney-Hasegawa-Mima model, focusing on the dynamics of spectral transfers and zonal flows. On the other hand, Ref. [27] explored the modulational instability in the Extended Hasegawa-Mima Equation, defining a key parameter that characterizes system behavior with changes in the Larmor radius.

The Hasegawa-Mima equation has also been examined in the context of curved magnetic fields as in Ref. [28]. Another paper, Ref. [29], which derived a HM equation for general magnetic configurations, serves as a fundamental model for studying turbulence in ion-electron plasmas, particularly where strong inhomogeneities in the magnetic field and electron density exist.

2.1.3 *Hasegawa-Mima Simulations*

On the computational front, various simulation algorithms have been developed for the Hasegawa-Mima equation. Finite element models have been proposed for the Hasegawa-Mima equation. For instance, Ref. [1] used a finite element

space-domain approach to semi-discretize the coupled variational Hasegawa–Mima model, demonstrating the global existence of solutions. Another simulation used Newton-type methods to simulate the HM model more efficiently [30].

Chapter 3

The Hasegawa-Mima Model

3.1 The Hasegawa-Mima Model for edge turbulence

Turbulence is an inherently unpredictable phenomenon, and this necessitates the formulation of a theory that addresses its statistical properties, ultimately yielding an estimate of average transport. In a tokamak, radial transport refers to the movement of particles, heat, or other quantities across the radial direction of the plasma. The radial direction is perpendicular to the magnetic field lines that confine the plasma. Turbulence in the plasma can cause particles and heat to be transported radially across the magnetic field lines. Controlling and minimizing radial transport is essential for maintaining the high temperatures and densities required for sustained fusion reactions. Therefore, a theory should be formulated to better understand turbulence in a tokamak. Drift waves typically arise in plasmas with density gradients perpendicular to the magnetic field. The presence of these gradients leads to the development of drift instabilities, and drift waves emerge as a result. These waves are driven by the curvature and gradient of the magnetic field.

In the subsequent sections, we derive a model equation for describing drift waves that contribute significantly to turbulence in the plasma. Our primary focus is acquiring a simplified model equation encompassing essential nonlinear dynamics. While this model might not allow for precise predictions of tokamak radial transport, it still provides valuable insights into simpler turbulent systems. This chapter delves into a detailed derivation of the Hasegawa-Mima equation, which is a reduced model for plasma turbulence. Specifically, the equation proves useful in describing the evolution of electrostatic potential fluctuations Φ or density fluctuations n.

Numerous efforts have been devised for the development of mathematical models describing plasma during its confinement to better understand the evolution of turbulence and instabilities. Solving the full Navier-Stokes equations (partial dif-

ferential equations that express the flow of viscous fluids) is complicated. Instead, a simpler model was developed by Hasegawa and Mima, leading to the so-called Hasegawa-Mima equation named after Akira Hasegawa and Kunioki Mima in 1977 to observe turbulence near the edge of tokamak plasmas. It is a non-linear equation useful in describing the evolution of electrostatic potential fluctuations Φ in a strongly magnetized plasma.

The Hasegawa-Mima model finds its applicability in the context of controlled nuclear fusion, where understanding and mitigating turbulent radial transport is critical for achieving the necessary conditions for sustained fusion reactions. As mentioned previously, fusion devices, such as tokamaks and stellarators, operate in regimes where turbulent transport can significantly impact plasma confinement and, thus, their overall performance. In fusion devices, where maintaining a high plasma temperature and density is essential for achieving fusion reactions, the control of turbulent transport becomes essential.

3.1.1 *On the Symmetry of a Tokamak*

We consider a cross-section of the tokamak and examine the density profile. Density is described as we move radially outwards from the core to the edge of the tokamak. The core region of the plasma, which is closer to the central axis of the torus, tends to have higher plasma density. As you move towards the edge of the plasma, the density may decrease.

The density profile may not be a simple monotonic function. It can have transitions and shapes tailored to optimize plasma stability, performance, and exhaust capabilities. However, according to both the Hasegawa-Mima and Hasegawa-Wakatani models, we consider the middle portion of the density profile where we have a non-zero gradient, and this is the shear or gradient region. This shear can be caused by a variation in density, electron or ion temperature, or current. The HM and HW models assume a linear middle portion and ignore the regions to the left and right where we have zero gradient. Thus, poloidal symmetry to the zeroth order is assumed, and the models only consider the radial density profile as shown in Figs. 3.1 and 3.2.

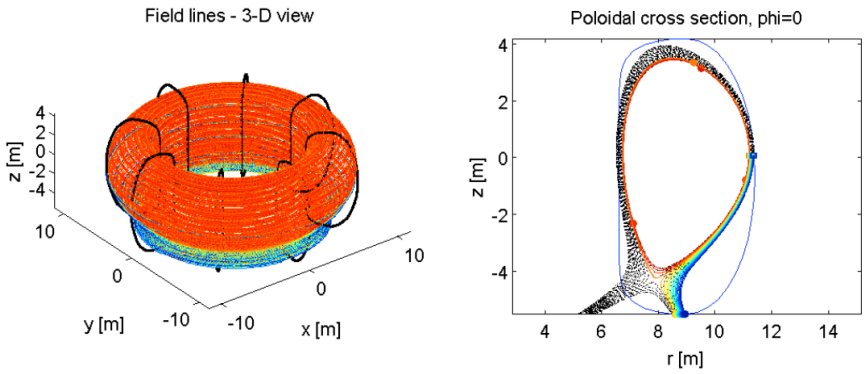

Figure 3.1: Magnetic Field Lines in a Tokamak

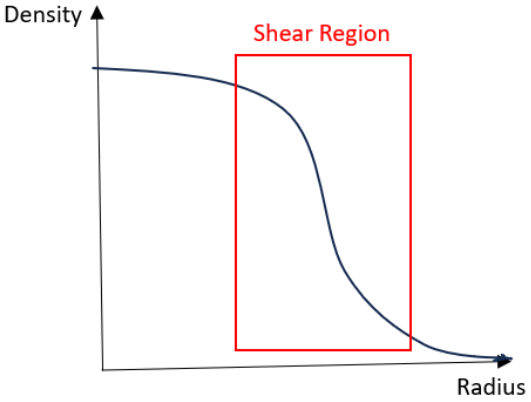

Figure 3.2: Density Profile

3.1.2 *Assumptions of the HM Model*

The assumptions of the Hasegawa-Mima model are enumerated below.

1. Uniform Magnetic Field and along the z-direction: $\vec{B} = B\hat{z}$. This means that the magnetic field does not vary spatially along the z-axis. Although the geometry of a tokamak shows that the presence of poloidal and toroidal magnetic fields necessitates non-uniformity, taking a small enough spatial region at the edge of the plasma, the magnetic field can be considered uniform along the z-direction, as shown in 3.1. The magnetic field in the tokamak is a result of current traversing poloidal and toroidal coils. Poloidal field coils carry a current in the poloidal direction. This current then induces a plasma current in the poloidal direction, which creates a magnetic field in

the toroidal direction according to the Biot-Savart law [31]

$$d\vec{B} = \frac{\mu_0}{4\pi} \frac{d\vec{I} \times (\vec{r} - \vec{r'})}{|\vec{r} - \vec{r'}|^3} \tag{3.1}$$

Assuming a uniform magnetic field along the z-direction implies poloidal and toroidal symmetry since the only variable under consideration is the radial direction. It is also important to note that the toroidal magnetic field is constant as it is generated by the toroidal field coils; however, the plasma current, which creates the poloidal magnetic field, fluctuates due to fluctuations in density and temperature. This fluctuation in current thus causes a fluctuation in the total magnetic field. To investigate the effect of plasma current fluctuations on the poloidal magnetic field B_θ, we consider an analogy to the situation.

We consider a toroidal coil around which a long wire is wrapped. The wire is wound in a uniform and tight enough manner that each turn can be considered a plane-closed loop. Assuming the cross-sectional area of the toroidal coil is rectangular, we attempt to obtain the expression of the magnetic field using the Biot-Savart law.

$$\begin{aligned} d\vec{B_\theta} &= \frac{\mu_0}{4\pi} \frac{d\vec{I} \times (\vec{r} - \vec{r'})}{|\vec{r} - \vec{r'}|^3} \\ &= \frac{\mu_0}{4\pi} \frac{\vec{I} \times \vec{\boldsymbol{\imath}}}{\hat{\boldsymbol{\imath}}^3} d\ell' \end{aligned} \tag{3.2}$$

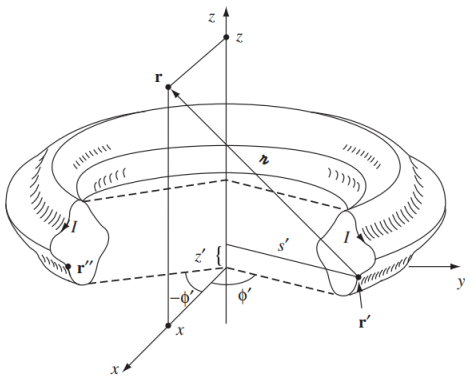

Figure 3.3: Toroidal Coil, adapted from [32]

Where $\vec{r}$ and $\vec{r'}$ are the position vectors of the point in space where the magnetic field is being measured and of the current element, respectively. And

we define $\vec{\boldsymbol{\imath}}$ to be $\vec{r}-\vec{r'}$.μ_0 is the permeability of free space $4\pi \times 10^{-7}$T m/A, I is the current flowing through the wire and $d\ell'$ is an infinitesimally small element of the wire carrying current. We consider $\vec{r}$ to be in the xz plane, so its Cartesian coordinates are $(x, 0, z)$, and the source coordinates of $\vec{r'}$ are $\vec{r'} = (s' \cos\Phi', s' \sin\Phi', z')$. Therefore, $\vec{\boldsymbol{\imath}} = (x - s\cos\phi, -s\sin\phi, z - z')$. The current does not have a Φ component, so $\vec{I} = I_s\hat{s} + I_z\hat{z}$, or in Cartesian coordinates, $\vec{I} = (I_s\cos\phi, I_s\sin\phi, I_z)$. Therefore,

$$\begin{aligned}\vec{I} \times \vec{\boldsymbol{\imath}} = &(\sin\phi\,(I_z(z - z') + sI_z))\,\hat{x} \\ &+ (I_z(x - s\cos\phi) - I_s\cos\phi(z - z'))\,\hat{y} + (-I_s x\sin\phi)\,\hat{z}.\end{aligned} \tag{3.3}$$

There is a symmetrical current element at $\vec{r}'$, with the same s, the same $\vec{r}$, $\vec{d\ell}'$, I_s, and I_z, but negative ϕ. $\sin\phi$ changes sign, so the $\hat{x}$ and $\hat{z}$ contributions from $\vec{r}$ and $\vec{r}'$ cancel out, leaving only a $\hat{y}$ term. Thus, the field at $\vec{r}$ is in the $\hat{y}$ direction, and in general, the field points in the $\hat{\phi}$ direction. We also know that the field is circumferential, so we apply Ampère's law to a circle of radius s about the axis of the toroid.

$$B \cdot 2\pi s = \mu_0 I_{\text{enclosed}}, \tag{3.4}$$

Hence,

$$\vec{B_\theta}(\vec{r}) = \begin{cases} \frac{\mu_0 NI}{2\pi s}\hat{\phi}, & \text{for points inside the coil,} \\ 0, & \text{for points outside the coil.} \end{cases} \tag{3.5}$$

Where N is the total number of turns.

Consider that the fluctuation in the current is a perturbation to it such that $I = I_0 + \delta I$. Substituting this into the obtained expression of the poloidal magnetic field

$$B_\theta = \frac{\mu_0 N(I_0 + \delta I)}{2\pi s}\hat{\phi} \tag{3.6}$$

therefore, based on the results obtained, a 1% perturbation to the current would mean that the poloidal magnetic field $\vec{B_\theta}$ is also perturbed by 1%

$$\frac{\delta B_\theta}{B_{0\theta}} = \frac{\delta I}{I} \tag{3.7}$$

2. The ions are assumed to be much colder than the electrons $T_i \ll T_e$, this allows us to treat ions as a cold fluid, which simplifies the equations at hand. This assumption is valid at the tokamak edge. According to ASDEX

Upgrade measurements of the electron and ion temperatures during an edge localized mode cycle, after the edge-localized mode (ELM) onset, the ion and electron temperatures increase close to the separatrix but decrease close to the edge [33]. However, there is a difference between the electron and ion temperature behavior at the onset of ELM. The electron temperature close to the separatrix remains unperturbed while the ion temperature increases. Another discrepancy in behavior is the recovery time for each of the two species. The maximum electron temperature gradient recovery after the ELM crash lasts about an entire inter-ELM period, while the ion temperature gradient is re-established much faster.

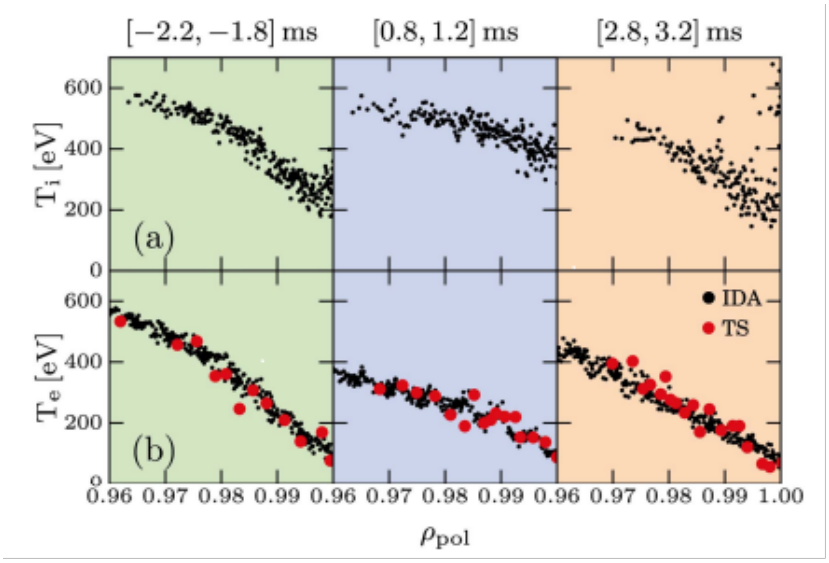

Figure 3.4: Electron and Ion Temperatures taken at three time periods in the ASDEX Upgrade Tokamak, adapted from [33]

Another set of ion and electron temperature measurements done on the DIII-D tokamak [34] shows that the ion temperature remains significantly higher than the electron temperature as the normalized radial coordinate $\rho = r/a$ increases.

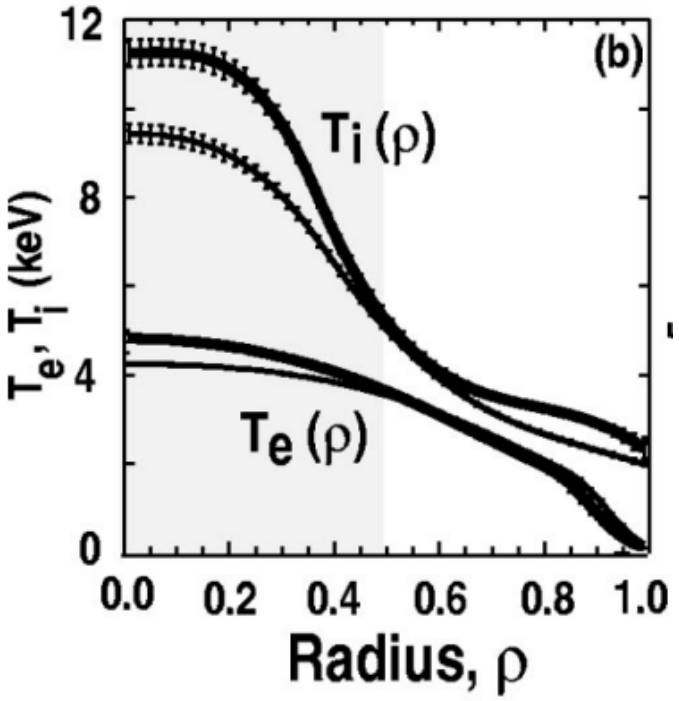

Figure 3.5: Radial Profile of Ion and Electron Temperatures, adapted from [34]

Another instance of such a recorded measurement in several limiter and divertor tokamaks is that $T_i > T_e$ in the scrape-off layer SOL [35]. This is due to the higher mobility of electrons compared to ions in the sheath SOL. These measurements highlight the limitations of the Hasegawa-Mima model and the discrepancy between experimental results and the assumptions of this model.

3. The plasma is considered to be quasi-neutral, meaning that the electron and ion charge densities are approximately equal $n_e \approx n_i$. Consequently, the net charge is zero for the first order. Assuming quasi-neutrality eliminates the need to consider the dynamics of individual ion and electron species. However, this assumption is only valid when the Debye length is much smaller than the characteristic length scales of the plasma. To put it in simpler terms, the scale over which ions and electrons influence each other's electrostatic potential in the plasma has to be much smaller than the scale of the experiment, which in this case is the tokamak. To the second order, though, one might consider a small deviation.

4. Constant electron temperature. The heat conservation equation, also known as the heat transport equation or energy balance equation, describes the

conservation of energy in a system, and it can be written as

$$\partial T/\partial t + \vec{\nabla}.\vec{q} = S \tag{3.8}$$

where T is the temperature, $\vec{q}$ is the heat flux vector, S is the heating source term, and $\vec{\nabla}.\vec{q}$ represents the divergence of the heat flux. Assuming a constant electron temperature, $\partial T_e/\partial t = 0$. This implies that the electron heat flux equals the heating source term S.

3.1.3 *Continuity Equation and Quasi-neutrality Assumption*

The continuity equations are fundamental equations that describe the conservation of the number of ions and electrons within a plasma. These equations emphasize that the total number of ions and electrons in a plasma volume is properly accounted for.

The equation essentially states that any change in particle density in a given region is balanced by the flux of particles into or out of that region. It ensures the conservation of the total number of ions within the plasma.

$$\frac{\partial n_i}{\partial t} + \vec{\nabla}_{\parallel}\left(n_i\vec{u}_i\right) + \vec{\nabla}_{\perp}\left(n_i\vec{u}_i\right) = 0 \tag{3.9}$$

n is the number density, $\vec{u}_i$ is the ion velocity, and $\partial n/\partial t$ represents the rate of change of density with respect to time. $\vec{\nabla}_{||}.(n_i\vec{u}_i)$ accounts for the divergence of the ion flux in the direction parallel to the magnetic field, while $\vec{\nabla}_{\perp}.(n_i\vec{u}_i)$ accounts for the divergence of the ion flux in the direction perpendicular to the magnetic field.

According to the quasi-neutrality assumption, the same equation is obtained for electrons. To assess the behavior of the density, we need to obtain the expressions for the ion and electron velocities. To do that, we must start with the ion- and electron-momentum balance equations.

3.1.4 *Electron Momentum Balance Equation*

$$n_e m_e \left(\frac{\partial \vec{u}_e}{\partial t} + (\overrightarrow{u}_e \cdot \vec{\nabla})\vec{u}_e\right) = -n_e e(\vec{E} + \overrightarrow{u}_e \times \vec{B}) - \vec{\nabla}p_e + n_e\nu_{ei}m_e(\overrightarrow{u}_e - \vec{u}_i) \tag{3.10}$$

Where:

n_e is the electron density,
m_e is the electron mass,
$\vec{u}_e$ is the electron velocity, and $\vec{u}_i$ is the ion velocity,
e is the electron charge,
$\vec{E}$ is the electric field,
$\vec{B}$ is the magnetic field,
$\vec{\nabla} p_e$ is the pressure gradient for electrons,
ν_{ei} is the electron-ion collision frequency.

The momentum balance equation for both ions and electrons is derived from Newton's second law. The left-hand side term comes from the convective derivative expression of the acceleration as the temporal derivative of velocity. The right-hand terms are the different forces acting on the particles in plasma. The first term of the momentum balance equation is $n_e m_e \left(\frac{\partial \vec{u}_e}{\partial t} + (\overrightarrow{u}_e \cdot \vec{\nabla}) \vec{u}_e \right)$ which represents the acceleration of electrons in the plasma. It includes the time derivative of electron velocity and the convective acceleration term. The second term $-n_e e(\vec{E} + \overrightarrow{u}_e \times \vec{B})$ represents Lorentz force, which is the force experienced by the electrons due to the combined effects of the electric field ($\vec{E}$) and the magnetic field ($\vec{B}$), along with the electron velocity ($\overrightarrow{u}_e$). The Lorentz force is due to the presence of a charged particle in the magnetic field in a tokamak. The third term, $-\vec{\nabla} p_e$, is the pressure gradient force, which is a force resulting from the spatial variation of pressure (p_e) within the system. This term is derived from a squared thermal velocity term, which, by the equipartition theorem, is associated with a $1/2 k_B T$ term. Then, using the ideal gas law, we express it in terms of pressure and thus obtain the pressure gradient term. The last term is the collisions or drag force term, $n_e \nu_{ei} m_e (\overrightarrow{u}_e - \vec{u}_i)$, which is a force arising from collisions between electrons and ions, characterized by the collision frequency (ν_{ei}), and the relative velocities of electrons ($\overrightarrow{u}_e$) and ions ($\vec{u}_i$). The collision term is due to the drag force caused by the electron-ion collisions, which causes a momentum loss upon different species colliding with each other.

3.1.5 *Properties of the HM Model Studied Analytically*

To evaluate the significance of each term, we first compare $\vec{u}_e \cdot \vec{\nabla} \vec{u}_e$ and $\vec{u}_e \times B$ from the Lorentz force term, and we then compare $n_e \nu_{ei} m_e (\vec{u}_e - \vec{u}_i)$ to $\vec{u}_e \times \vec{B}$.

$$\frac{n_e m_e \left(\vec{u}_e \cdot \vec{\nabla}\right) \vec{u}_e}{n_e e \left(\vec{u}_e \times \vec{B}\right)} \sim \frac{m_e u_e^2 / L}{e u_e B} = \frac{m_e}{e} \frac{u_e}{LB} = \frac{\rho_s}{L} \tag{3.11}$$

Where L is the characteristic scale length, and ρ_s is the Larmor radius defined as

$$\rho_s = mu/eB$$

The ratio we obtain is unitless and can be understood as an effective Reynolds number. The effective Reynolds number is a dimensionless quantity which helps predict some properties of the dynamics in different situations, by measuring the ratio between inertial and viscous forces [36]. If $\rho_s/L \ll 1$ then, $\rho_s \ll L$, then the Larmor radius, which is the radius of the circular motion of a charged particle, is much less than the characteristic scale length, which can be related to the size of the experiment or device being dealt with. On the other hand, if $\rho_s/L \gg 1$ then $\rho_s \gg L$, then the Larmor radius is much greater than the scale length.

Another effective Reynolds number can be obtained by comparing $n_e \nu_{ei} m_e (\vec{u}_e - \vec{u}_i)$ to $\vec{u}_e \times \vec{B}$.

$$\frac{n_\alpha m_\alpha \nu_{\alpha\beta} \left(\vec{u}_\alpha - \vec{u}_\beta\right)}{n_\alpha e_\alpha \left(\overrightarrow{u_\alpha} \times \vec{B}\right)} = \frac{m_\alpha}{e_\alpha} \frac{\nu_{\alpha\beta} \left|\vec{u}_\alpha - \vec{u}_\beta\right|}{u_\alpha B} = \frac{m_\alpha}{e_\alpha} \frac{\nu_{\alpha\beta}}{B} = \frac{\nu_{\alpha\beta}}{\omega_{c,\alpha}} \tag{3.12}$$

where $\omega_{c,\alpha}$ is the cyclotron frequency of particle α: $\omega_{c,\alpha} = \frac{e_\alpha B}{m_\alpha}$

If $\frac{\nu_{\alpha\beta}}{\omega_{c,\alpha}} \ll 1$ then, $\nu_{\alpha\beta} \ll \omega_{c,\alpha}$. In this case, the frequency at which particles are rotating is much larger than the collision frequency. On the other hand, if $\frac{\nu_{\alpha\beta}}{\omega_c} \gg 1$ then, $\nu_{\alpha\beta} \gg \omega_{c,\alpha}$. Then, the collision frequency is greater than the cyclotron frequency.

3.1.6 *Deriving the HM Model*

Based on the above analysis of effective Reynolds numbers and the Hasegawa-Mima paper written in 1977 [21], we can derive the HM model. We ignore the first and third terms, as they are less significant than the second term. Thus, the electron momentum balance equation becomes:

$$-n_e e \left(\vec{E} + \overrightarrow{u_e} \times \vec{B}\right) - \vec{\nabla} p_e = 0 \tag{3.13}$$

Projecting the parallel and perpendicular components of the electron momentum balance equation;

$$-n_e e \left(\vec{E}_\parallel + (\overrightarrow{u_e} \times \vec{B})_\parallel\right) - \vec{\nabla}_\parallel p_e = 0 \tag{3.14}$$

$$-n_e e\left(\vec{E}_\perp + (\overrightarrow{u_e} \times \vec{B})_\perp\right) - \vec{\nabla}_\perp p_e = 0 \tag{3.15}$$

But if $\vec{E} = -\vec{\nabla}\Phi$, and $p_e = n_e T_e$ according to the ideal gas law, and assuming T_e is constant, the momentum balance equation becomes

$$\vec{0} = -n_e e\left(-\vec{\nabla}_\parallel \Phi + \left(\vec{u}_e \times \vec{B}\right)_\parallel\right) - T_e \vec{\nabla}_\parallel n_e \tag{3.16}$$

But $(\vec{u}_e \times \vec{B})_\parallel = 0$ therefore;

$$n_e e\vec{\nabla}_\parallel \Phi - T_e \vec{\nabla}_\parallel n_e = 0 \tag{3.17}$$

Re-ordering the terms of the equation and integrating with respect to z:

$$\begin{aligned} &T_e \vec{\nabla}_\parallel n_e = n_e e \vec{\nabla}_\parallel \Phi \\ &\Rightarrow n_e = n_{e0} e^{\frac{e\Phi}{T_e}} \text{ Boltzmann Relation} \end{aligned} \tag{3.18}$$

Now, we introduce a first-order perturbation to the particle density such that $n_e = n_{e0} + \delta n_e$, and a first-order perturbation to the electrostatic potential such that $\Phi = 0 + \Phi$

$$\begin{aligned} &n_e = n_{e_0} e^{\frac{e\Phi}{T_e}} \\ &\frac{n_{e_0} + \delta n_e}{n_{e_0}} = e^{\frac{e\Phi}{T_e}} \\ &\Rightarrow \frac{\delta n_e}{n_{e_0}} = \frac{e\Phi}{T_e} \text{ Adiabatic Response of Electrons} \end{aligned} \tag{3.19}$$

The adiabatic response of electrons, which is a linearization of the Boltzmann relation, expresses that a change in the electron density δn_e with respect to the initial electron density n_{e_0} is proportional to Φ, and this proportionality is strict in the case where we neglect collision s as in the HM model. Therefore, when there is a perturbation, there is no delay in the response between the electron and electrostatic potential responses, and the two responses are said to be in phase.

Now, we move on to the ion momentum balance equation, similar to the electron momentum balance equation;

$$n_i m_i \left(\frac{\partial \vec{u}_i}{\partial t} + \left(\overrightarrow{u}_i \cdot \vec{\nabla}\right)\overrightarrow{u}_i\right) = n_i e\left(\vec{E} + \vec{u}_i \times \vec{B}\right) - \vec{\nabla} p_i + n_i \nu_{ie} m_i \left(\overrightarrow{u}_i - \vec{u}_e\right) \tag{3.20}$$

We also ignore the collision term due to the same comparison done for the electron momentum balance equation.

$$n_i m_i \frac{d\vec{u}_i}{dt} = n_i e\left(\vec{E} + \vec{u}_i \times \vec{B}\right) + n_i \nu_{ie} m_i \left(\vec{u}_i - \vec{u}_e\right) \tag{3.21}$$

Applying the cold ions assumption $T_i \ll T_e$, we obtain:

$$\frac{d\vec{u}_i}{dt} = \frac{e}{m_i}\vec{E} + \frac{e}{m_i}\left(\overrightarrow{u_i} \times \vec{B}\right) \tag{3.22}$$

Electrons	Ions
$\vec{u}_{e\perp} = 0$	$\vec{u}_{i\perp} \neq 0$
$\vec{u}_{e\parallel} \neq 0$	$\vec{u}_{i\parallel} = 0$

Parallel motion is the motion along the magnetic field (in the z-direction), and the inertia of each particle species dictates it. Due to electrons being lighter than ions, their motion dominates in the parallel direction. Whereas the motion in the direction perpendicular to the magnetic field is composed of the $\vec{E} \times \vec{B}$ drift and the polarization drift. The polarization drift (also referred to as the inertia drift) is mass-dependent, so it can be ignored for electrons.

So, we take the perpendicular component of the ion momentum balance equation and apply perturbation theory to express the perpendicular ion velocity.We divide the equation by $m_i n_i$, to get:

$$\begin{aligned} \frac{d\vec{u}_{i\perp}}{dt} &= \frac{e}{m_i}\vec{E}_\perp + \frac{e}{m_i}\left(\vec{u}_i \times \vec{B}\right)_\perp \\ \vec{u}_{i\perp} &= \vec{u}^0_{i\perp} + \vec{u}^1_{i\perp} + \dots \end{aligned} \tag{3.23}$$

Linearizing the equation to the zeroth order:

$$\begin{aligned} 0 &= \frac{e}{m_i}\vec{E}_\perp + \frac{e}{m_i}\left(\vec{u}^0_{i\perp} \times \vec{B}\right)_\perp \\ 0 &= \vec{E}_\perp \times \vec{B} + \left(\vec{u}^0_{i\perp} \times \vec{B}\right)_\perp \times \vec{B} \\ -\vec{E}_\perp \times \vec{B} &= \left(\vec{u}^0_{i\perp} \times \vec{B}\right) \times \vec{B} \\ \vec{\nabla}_\perp \Phi \times \vec{B} &= (\vec{u}^0_{i\perp} \cdot \vec{B})\vec{B} - (\vec{B} \cdot \vec{B})\vec{u}^0_{i\perp} \end{aligned} \tag{3.24}$$

So, $\vec{u}^0_{i\perp} = \vec{u}_E = \frac{\vec{E}\times\vec{B}}{B^2} = -\frac{\vec{\nabla}\Phi\times\vec{B}}{B^2}$, which is the $\vec{E} \times \vec{B}$ drift $\vec{u}_E$ Similarly, from first-order linearization,

$$\begin{aligned} &\vec{u}_{i\perp} = \vec{u}^0_{i\perp} + \vec{u}^1_{i\perp} + \dots \\ &m_i n_i \frac{d}{dt}\left(\vec{u}^0_{i\perp} + \vec{u}^1_{i\perp}\right) = e n_i \left(\vec{E}_\perp + \left(\left(\vec{u}^0_{i\perp} + \vec{u}^1_{i\perp}\right)_\perp \vec{B}\right)_\perp\right) \\ &m_i n_i \frac{d}{dt}\vec{u}^0_{i\perp} + m_i n_i \frac{d\vec{u}^1_{i\perp}}{dt} = e n_i \vec{E}_\perp + e n_i \left(\left(\vec{u}^0_{i\perp} \times \vec{B}\right)_\perp + \left(\vec{u}^1_{i\perp} \times \vec{B}\right)_\perp\right) \end{aligned} \tag{3.25}$$

but, $0 = \vec{E}_\perp \times \vec{B} + \left(\vec{u}^0_{i\perp} \times \vec{B}\right) \times \vec{B}$ (obtained from 0^{th} order term)

Now, we drop 3^{rd} order (or higher) terms

$$\begin{aligned} m_i n_i \frac{d\vec{u}^0_{i\perp}}{dt} &= e n_i \left(\vec{u}^1_{i\perp} \times \vec{B}\right)_\perp \\ \text{so, } \left(\vec{u}^1_{i\perp} \times \vec{B}\right)_\perp &= \frac{m_i}{e}\left[\frac{\partial \vec{u}^0_{i\perp}}{\partial t} + \left(\vec{u}^0_{i\perp} \cdot \vec{\nabla}\right)\vec{u}^0_{i\perp}\right] \end{aligned} \tag{3.26}$$

$$\vec{u}^1_{i\perp} = \vec{u}_p = \frac{1}{\omega_{ci} B}\frac{d\vec{E}_\perp}{dt} = -\frac{1}{\omega_{ci} B}\frac{d\vec{\nabla}_\perp \Phi}{dt}$$

This obtained velocity is the polarization drift, which is the drift caused by a varying electric field. It is charge-dependent, so ions and electrons drift in opposite directions. It's also mass-dependent, so since $m_i \gg m_e$, this drift can be neglected for electrons. Now, we plug in the $\vec{E} \times \vec{B}$ drift $\vec{u}_E$ and the polarization drift $\vec{u}_p$ into the ion continuity equation.

$$\begin{aligned} &\frac{\partial}{\partial t} n_i + \vec{\nabla} \cdot (n_i \vec{u}_i) = 0 \\ &\frac{\partial n_i}{\partial t} + \vec{\nabla}_\parallel (n_i \vec{u}_i) + \vec{\nabla}_\perp (n_i \vec{u}_i) = 0 \\ &\frac{\partial n_i}{\partial t} + \vec{\nabla}_\parallel \left(n_i \left(\vec{u}_{i\parallel} + \vec{u}_{i\perp}\right)\right) + \vec{\nabla}_\perp \left(n_i \left(\vec{u}_{i\parallel} + \vec{u}_{i\perp}\right)\right) = 0 \\ &\frac{\partial n_i}{\partial t} + \vec{\nabla}_\perp (n_i \vec{u}_{i\perp}) = 0 \\ &\frac{\partial n_i}{\partial t} + \vec{\nabla}_\perp (n_i \vec{u}_E) + \vec{\nabla}_\perp (n_i \vec{u}_p) = 0 \end{aligned}$$

$$\frac{\partial n_i}{\partial t} + \vec{u}_E \vec{\nabla}_\perp n_i + n_i \vec{\nabla}_\perp \vec{u}_p = 0$$

* $\vec{\nabla}_\perp \cdot \vec{u}_p \neq 0$ to ensure compressibility (change in ion density such that quasi-neutrality is satisfied) Adding a first-order perturbation to density and dividing by n_{i0}

$$\begin{aligned} &\tfrac{1}{n_{i0}}\tfrac{\partial}{\partial t}(\delta n_i) + \tfrac{\vec{u}_E}{n_{i0}}\vec{\nabla}_\perp n_{i0} + \vec{\nabla}_\perp \vec{u}_p = 0 \qquad \tfrac{\partial_t n_{i0}}{n_{i0}} = \tfrac{\partial_t\left(\frac{n_{i0}}{\omega_{ci}}\right)}{\frac{n_{i0}}{\omega_{ci}}} = \partial_t \ln\left(\tfrac{n_{i0}}{\omega_{ci}}\right) \\ &\tfrac{\partial}{\partial t}\left(\tfrac{\delta n_i}{n_{i0}}\right) + \vec{u}_E \vec{\nabla}_\perp \ln\left(\tfrac{n_{i0}}{\omega_{ci}}\right) + \vec{\nabla}_\perp \vec{u}_p = 0 \end{aligned}$$

But $\frac{\delta n_i}{n_{i0}} = \frac{e\Phi}{T_e}$ (assuming quasi-neutrality)

and $\vec{u}_p = \frac{1}{\omega_i B}\left(-\frac{\partial}{\partial t}\vec{\nabla}_\perp \Phi\right)$

$$\frac{\partial}{\partial t}\left(\frac{\delta n_i}{n_{i0}}\right) + \vec{\nabla}_\perp \frac{1}{\omega_{ci}B}\left(-\frac{\partial}{\partial t}\vec{\nabla}_\perp \Phi\right) + \vec{u}_E \cdot \vec{\nabla}_\perp \ln\left(\frac{n_0}{\omega_{ci}}\right) = 0$$
$$\frac{\partial}{\partial t}\left(\frac{e\Phi}{T_e}\right) - \frac{1}{\omega_{ci}B}\frac{\partial}{\partial t}\left(\vec{\nabla}_\perp^2 \Phi\right) + \vec{u}_E \cdot \vec{\nabla}_\perp \ln\left(\frac{n_0}{\omega_{ci}}\right) = 0$$
$$\frac{\partial}{\partial t}\left(\frac{1}{\omega_{ci}B}\vec{\nabla}_\perp^2 \Phi - \frac{e\Phi}{T_e}\right) + \left(\vec{u}_E \cdot \vec{\nabla}_\perp\right) \ln\left(\frac{n_0}{\omega_{ci}}\right) = 0$$

Which is the unnormalized Hasegawa-Mima Equation

To Normalize: $\omega_{ci} t \to t \quad , \quad \frac{x,y}{\rho_s} \to x, y \quad , \quad \frac{e\Phi}{T_e} \to \Phi$

where $\rho_s = \sqrt{\frac{T_e}{m_i}}\frac{1}{\omega_{ci}}$

$$\frac{\partial}{\partial t}\left(\vec{\nabla}_\perp^2 \Phi - \Phi\right) - \left[\left(\vec{\nabla}_\perp \Phi \times \hat{z}\right) \cdot \vec{\nabla}_\perp\right]\left[\vec{\nabla}_\perp^2 \Phi - \ln\left(\frac{n_0}{\omega_c}\right)\right] = 0$$

Chapter 4

Analytical Approaches to the HM Model

In this chapter, we aim to study the HM model analytically, through first obtaining an effective Reynolds number to understand the dynamics for different cases and then focusing on the linear term of the HM equation. Firstly, we will obtain the HM drift wave dispersion relation for the linear case, then we will choose a form of Φ that eventually allows us to generalize for an expression of white noise with a constant amplitude. This will lead us to understand the evolution of white noise under the HM model, and the role that the linear term of this equation plays in the evolution.

As derived in Chapter 3, the Hasegawa-Mima Equation expressed using Poisson brackets is

$$\partial_t(\vec{\nabla}^2\Phi - \Phi) = \{\vec{\nabla}^2\Phi, \Phi\} + \{\Phi, ln(\frac{n_0}{\omega_{ci}})\} \tag{4.1}$$

Where $\{\vec{\nabla}^2\Phi, \Phi\}$ is the non-linear term, and $\{\Phi, \ln\left(\frac{n_0}{\omega_{ci}}\right)\}$ is the linear term.

To derive the effective Reynolds number of this equation, we first manipulate each of the nonlinear and linear terms, expressing Φ using Fourier modes such that $\Phi(x, y, t) = \Phi e^{i(k_x x + k_y y - \omega t)}$.

Starting with the nonlinear term

$$\{\Phi, \vec{\nabla}^2\Phi\} = (\frac{\partial\Phi}{\partial x})(\frac{\partial}{\partial y}\vec{\nabla}^2\Phi) = k_x k_y^3 \Phi^2 \tag{4.2}$$

And the linear term, assuming that n_0 is y-dependent

$$\{\Phi, ln(\frac{n_0}{\omega_{ci}})\} = (\frac{\partial\Phi}{\partial x})(\frac{\partial}{\partial y} ln(\frac{n_0}{\omega_{ci}})) = \frac{k_x\Phi}{L_n} \tag{4.3}$$

Where $L_n^{-1} = \partial_y(ln(n_0)) = \partial_y n_0/n_0$

Therefore, the effective Reynolds number R is

$$R = \frac{k_x k_y^3 \Phi^2}{k_x \Phi / L_n} = L_n k_y^3 \Phi \tag{4.4}$$

To get an estimate of the value of R, we consider $L_n \approx 100$, $k \approx 10$, and $\Phi \approx 10^{-3}$. Therefore, $R = 100$, indicating a dominance of the nonlinear term in such a regime.

4.1 HM Drift Wave Dispersion Relation

Drift waves are instabilities that arise in the plasma due to the presence of density gradients. The HM model can be modified to give us some insight into the behavior of drift waves. We can express the Hasegawa-Mima equation in terms of Poisson brackets:

$$\partial_t(\vec{\nabla}^2\Phi - \Phi) = \{\vec{\nabla}^2\Phi, \Phi\} + \{\Phi, ln(\frac{n_0}{\omega_{ci}})\} \tag{4.5}$$

Where $\{\vec{\nabla}^2\Phi, \Phi\}$ is the non-linear term, and $\{\Phi, \ln\left(\frac{n_0}{\omega_{ci}}\right)\}$ is the linear term.

4.2 Linear HM Equation

If we neglect the nonlinear term:

$$\begin{aligned} \partial_t\left(\vec{\nabla}^2\Phi - \Phi\right) &= \left\{\Phi, \ln\left(\frac{n_o}{\omega_{ci}}\right)\right\} \\ \partial_t\left(\vec{\nabla}^2\Phi - \Phi\right) &= \frac{\partial\Phi}{\partial x}\frac{\partial}{\partial y}\left(\ln\left(\frac{n_o}{\omega_{ci}}\right)\right) - \frac{\partial\Phi}{\partial y}\frac{\partial}{\partial x}\ln\left(\frac{n_0}{\omega_{ci}}\right)\Big) \end{aligned} \tag{4.6}$$

This makes the linear HM equation in one dimension

$$\begin{aligned} \frac{\partial}{\partial t}(\frac{\partial^2\Phi}{\partial x^2} - \Phi) &= \frac{\partial\Phi}{\partial x}\frac{\partial}{\partial y}ln(n_0) \\ \frac{\partial}{\partial t}(\frac{\partial^2\Phi}{\partial x^2} - \Phi) &= \frac{\partial\Phi}{\partial x}\frac{1}{L_n} \end{aligned} \tag{4.7}$$

Expressing Φ in terms of Fourier modes and plugging back into the above equation:

$$\begin{aligned} i\omega k_\perp^2\Phi + i\omega\Phi &= -ik_x\Phi\frac{1}{L_n} \\ i\omega\left(k_\perp^2 + 1\right) &= -ik_x\frac{1}{L_n} \end{aligned} \tag{4.8}$$

$$\omega = \frac{-k_x L_n^{-1}}{1 + k_\perp^2} \tag{4.9}$$

which is the drift wave dispersion relation. This result indicates the presence of a convective velocity caused by the gradient of the $ln(n_0)$ term.

4.3 Studying the evolution of a one-dimensional sinusoidal ϕ

As mentioned in EQ. 4.7, the linear HM equation in one-dimension is

$$\frac{\partial}{\partial t}(\frac{\partial^2 \phi}{\partial x^2} - \phi) = \frac{\partial \phi}{\partial x}\frac{1}{L_n} \tag{4.10}$$

Where $L_n = \partial_y n_0 / n_0$

We consider ϕ to be of the form $\phi(x,t) = \Phi(x,t)\sin(k_x x)$, and we assume that

$$\frac{1}{\Phi}\frac{\partial \Phi}{\partial x} \ll \ k_x$$

which means that Φ has a slowly varying amplitude with respect to x, in comparison with the sine wave. Therefore $\partial_x \phi \approx \Phi \cos(k_x x)$. Plugging this form of ϕ into the HM equation, and applying the assumptions, we obtain

$$\frac{\partial_t \Phi(x,t)}{\Phi(x,t)} = -\frac{1}{L_n}\frac{k_x}{k_x^2 + 1}\frac{\cos(k_x x)}{\sin(k_x x)} \tag{4.11}$$

Integrating both sides with respect to time gives

$$ln(\Phi(x,t)) = -\frac{1}{L_n}\frac{k_x}{k_x^2 + 1}\frac{\cos(k_x x)}{\sin(k_x x)}t \tag{4.12}$$

therefore

$$\Phi(x,t) = e^{\lambda(x)t} \tag{4.13}$$

Where

$$\lambda(x) = -\frac{1}{L_n}\frac{k_x}{k_x^2 + 1}cot(k_x x) \tag{4.14}$$

It is also worth looking into the nonlinear term of the Hasegawa-Mima equation for the form of ϕ, which we have chosen $\phi(t) = \Phi(x,t)\sin(k_x x)$.

$$\{\vec{\nabla}^2\phi, \phi\} = \frac{\partial}{\partial x}(\vec{\nabla}^2\phi)(\frac{\partial}{\partial y}\phi) - \frac{\partial}{\partial y}(\vec{\nabla}^2\phi)\frac{\partial}{\partial x}\phi = 0 \tag{4.15}$$

Therefore, to study the effect of the nonlinear term on the evolution of ϕ, we would need to choose a ϕ dependent on both x and y, so the nonlinear term is nonzero.

4.4 Studying the Evolution of White Noise

Background noise is an inherent characteristic of physical systems. White noise, in particular, serves as an idealized initial condition that simulates the statistical properties of random noise. White noise is a random signal having equal intensity at different frequencies, such that $\Phi = \sum \Phi_j(t) exp(ik_j x)$.

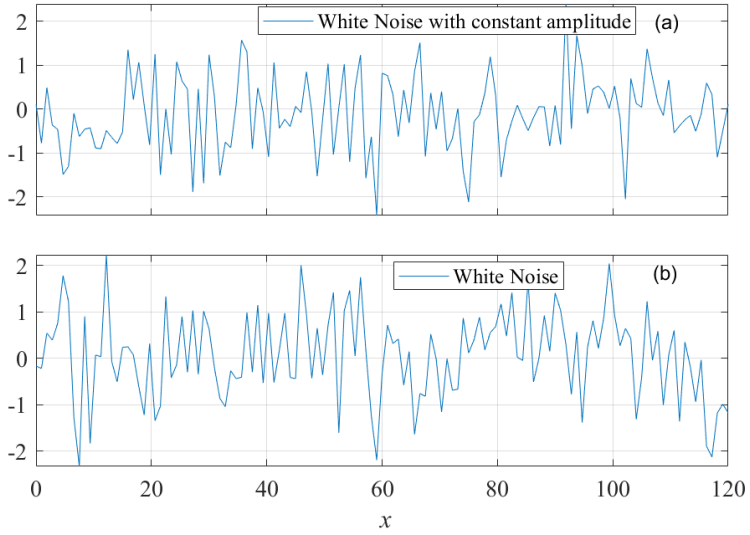

Figure 4.1: White noise vs. x

In an attempt to study the effect of gradients in the density profile on background noise, the following choice of Φ is taken

$$\phi(x,t) = \Phi_1(x,t)\sin(k_1 x) + \Phi_2(x,t)\sin(k_2 x) \tag{4.16}$$

where $\Phi_1(x,t)$ is the amplitude of the first sine wave, and $\Phi_2(x,t)$ is the amplitude of the second. The two sine waves have different wavenumbers k_1 and k_2. The above choice of ϕ is only x-dependent because this produces a zero nonlinear term in the HM equation.

We assume ϕ is of the form

$$\phi(x,t) = \Phi_1(x,t)\sin(k_1 x) + \Phi_2(x,t)\sin(k_2 x) \tag{4.17}$$

If $k_1 \neq k_2$ but $k_1 \sim k_2$, and assuming all modes have the same amplitude for simplicity such that $\Phi_1(x,t) = \Phi_2(x,t) = \Phi(x,t)$.

Taking $\phi = \Phi(x,t)\,(\sin(k_1 x) + \sin(k_2 x))$, and assuming that

$$\frac{1}{\Phi}\frac{\partial \Phi}{\partial x} \ll k_1 \text{ and } \frac{1}{\Phi}\frac{\partial \Phi}{\partial x} \ll k_2$$

We plug the above form of ϕ into the linear HM equation 4.7, and we obtain

$$\Phi(x,t) = e^{\lambda(x)t} \tag{4.18}$$

Where

$$\lambda(x) = \frac{-1}{L_n} \frac{k_1 \cos(k_1 x) + k_2 \cos(k_2 x)}{(k_1^2+1)\sin(k_1 x) + (k_2^2+1)\sin(k_2 x)} \tag{4.19}$$

Generalizing to k_i

$$\lambda(x) = -\frac{1}{L_n} \frac{\sum k_i \cos(k_i x)}{\sum (k_i^2+1)\sin(k_i x)} \tag{4.20}$$

This simulates random noise in the x direction.

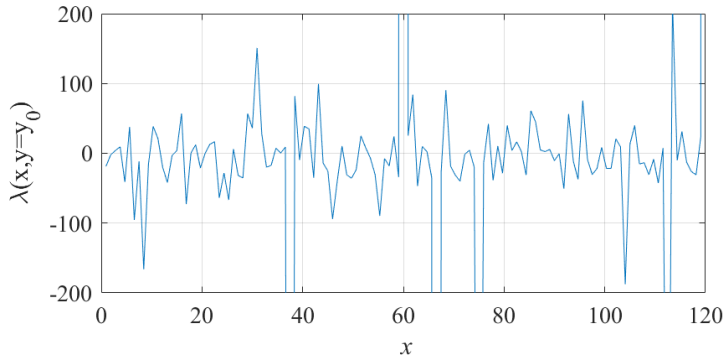

Figure 4.2: Sum of λ vs. x for all values of k ranging from 0 to 2π

It is evident that λ has a positive component. Therefore, Φ grows with time. The increase in the amplitude of Φ is not caused by instability but rather by a positive λ resulting from dynamics imposed by the linear term in the HM equation.

Chapter 5

Hasegawa-Mima Numerical Simulation

To simulate the Hasegawa-Mima model, we use the finite-element model. The simulations presented were conducted using FreeFEM++, an open-source finite element software designed for solving partial differential equations (PDEs). FreeFEM++ provides a high-level scripting language that allows for flexible meshing, complex geometries, and efficient numerical solvers.

In this work, FreeFEM++ was utilized to solve the governing equations of the system, implement boundary conditions, and generate high-resolution computational meshes. The simulation parameters, mesh structure, and numerical schemes are detailed in the following sections.

The method described in [1] relies on first expressing the Hasegawa-Mima model in terms of Poisson brackets and then formulating it as a coupled system of linear hyperbolic-elliptic partial differential equations that will be easier to deal with using a Finite Element scheme for obtaining a numerical approximation. Additionally, the simulation is formulated within a Variational frame obtained through full discretization. To state it briefly, the HM model is reduced to a set of matrix equations with periodic boundary conditions, which are then solved over a specified mesh grid through the algorithm.

5.1 Scaling According to Normalization Factors

As discussed at the end of section 3.1.6, both the spatial and temporal scales in the HM model are normalized by different factors, which reflects on our choice of parameters for the simulation.

The time scale is normalized such that $t_{simulation} = \omega_{ci} t_{real}$, which means that when we run our simulation for a 1000 timesteps, we are running it for 10^{-4} seconds

in real-time.

As for the spatial scale, our choice of x and y limits, are such that $x_{simulation}$ or $y_{simulation} = [0, \frac{x_{real}}{\rho_s}]$. This matter of normalization gives us a direct interpretation of how our parameters scale in real life and experimentally.

5.2 Simulating the Temporal Evolution of White Noise in Slab Geometry

The simulation uses the finite element method, where the Hasegawa-Mima equation is first derived into its variational form and then expressed in FreeFEM++ [37]. The spatial domain is set, and a mesh is applied with a specific number of mesh or grid points. The number of mesh points is 128. The total length in the x and y directions is respectively 120 and 80, yielding resolutions about 0.9 and 0.6 ρ_s as shown in 5.1 .

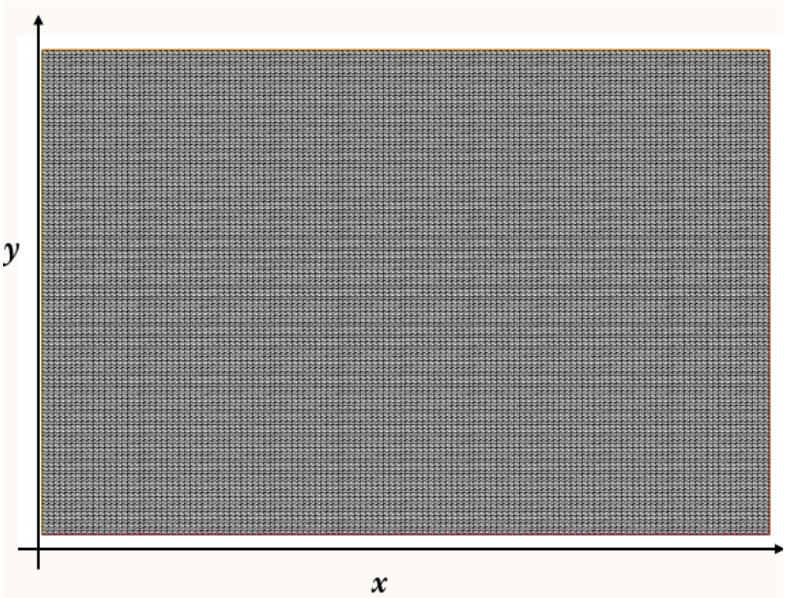

Figure 5.1: Mesh generated using FreeFEM++ for the slab geometry case

Neumann boundary conditions are used in the x-direction (equivalent to the radial direction) and periodic in the y-direction (equivalent to the poloidal direction) as shown in 5.2.

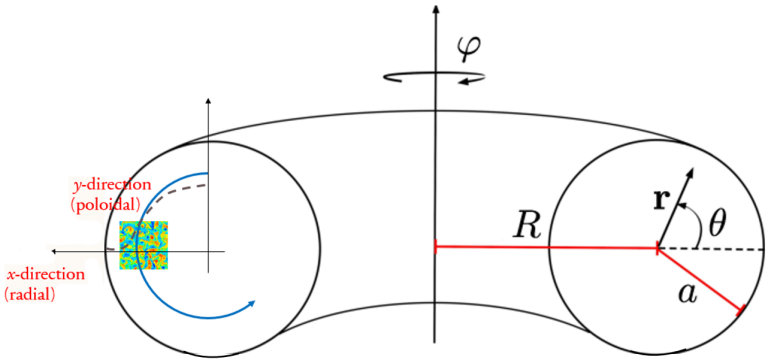

Figure 5.2: Cross-section of a tokamak depicting the spatial scale under study

5.2.1 *Initial Conditions for* Φ

Based on the choice of an initial condition that simulates white noise such that $\Phi(x, y, t = 0) = 10^{-3} \sum_i \sum_j \Phi_{ij} \sin(k_i x) \sin(k_j y)$, Φ is shown in the figure below.

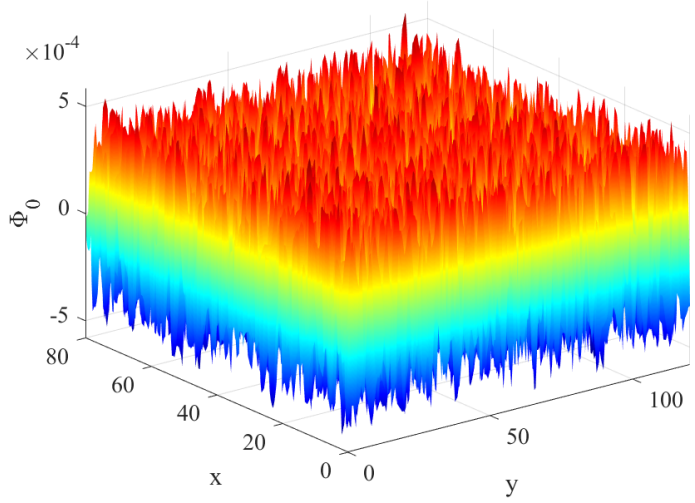

Figure 5.3: Initial condition Φ

Since the edge region of a tokamak is being simulated, this necessitates periodicity in one direction; however, the other direction is not necessarily periodic. In this simulation, Neumann boundary conditions are applied in the x-direction and periodic boundary conditions in the y-direction.

5.2.2 *Choice of* n_0

To study the effect of the density gradient on the evolution of Φ, the form of the density profile n_0 is a one-dimensional hyperbolic tangent function, such that $n_0 = 1 + \epsilon + tanh(\kappa(y - a))$, where ϵ is taken to be 10^{-10} and it determines the width of the gradient region, κ is the steepness, a is the position of maximum gradient. a is taken to be equal to 55 for all runs, while κ is varied between 0.25 and 1.9. n_0 is shown in the figure below, in addition to K_y which is $\frac{\partial}{\partial y} log(\frac{n_0}{\omega_{ci}})$

Given the above choice of n_0, the following expression of K_y is obtained

$$K_y = \frac{\kappa \, \mathrm{sech}(\kappa(y-a))}{1 + \epsilon + \tanh(\kappa(y-a))} \tag{5.1}$$

or

$$K_y = \frac{\kappa}{[\cosh^2(\kappa(y-a))][1 + \epsilon + \tanh(\kappa(y-a))]} \tag{5.2}$$

This highlights the dependence of the gradient region on ϵ. For $\epsilon \ll 1$, as ϵ increases, the width of the gradient region decreases.

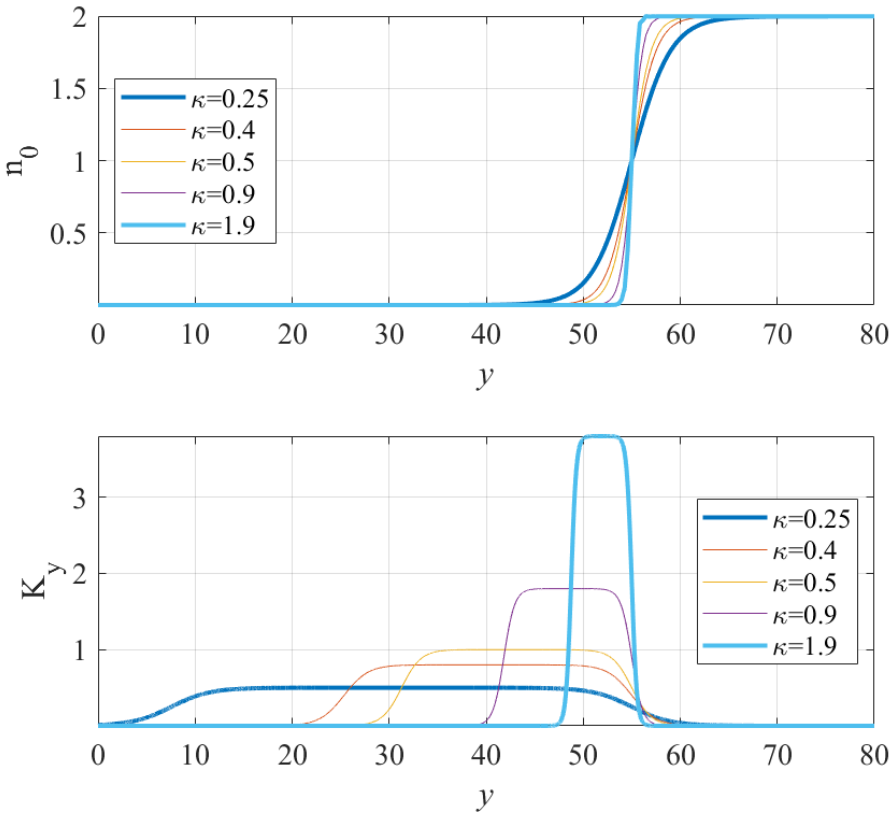

Figure 5.4: Variation of n_0 and K_y versus y

Steepness κ	Run time
0.2	447
0.25	288
0.3	215
0.4	124
0.5	83
0.7	46
0.9	32
1.1	23
1.3	19
1.5	16
1.7	14
1.9	13

Table 5.1: Variation of Run time as a function of steepness κ

A cutoff amplitude of 0.3 is imposed. As the steepness κ increases, the run time decreases, and the cutoff amplitude is reached much faster. As the steepness κ increases, the cutoff time decreases.

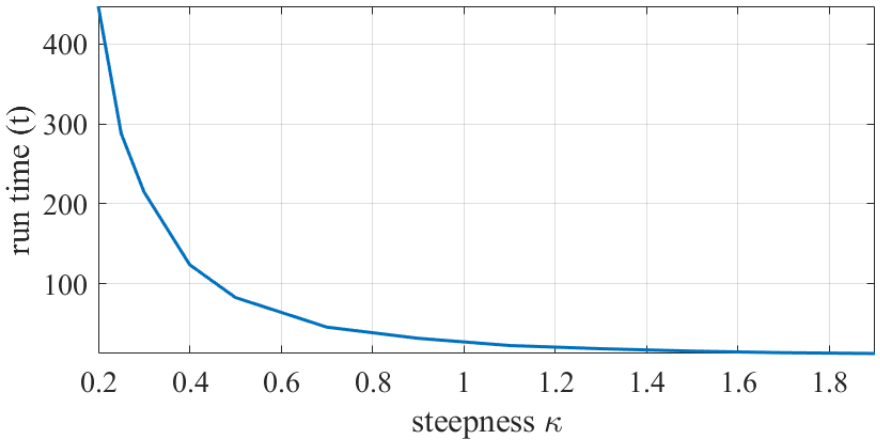

Figure 5.5: Run time t as a function of steepness κ

5.2.3 *The spatial and temporal evolution of the electrostatic potential*

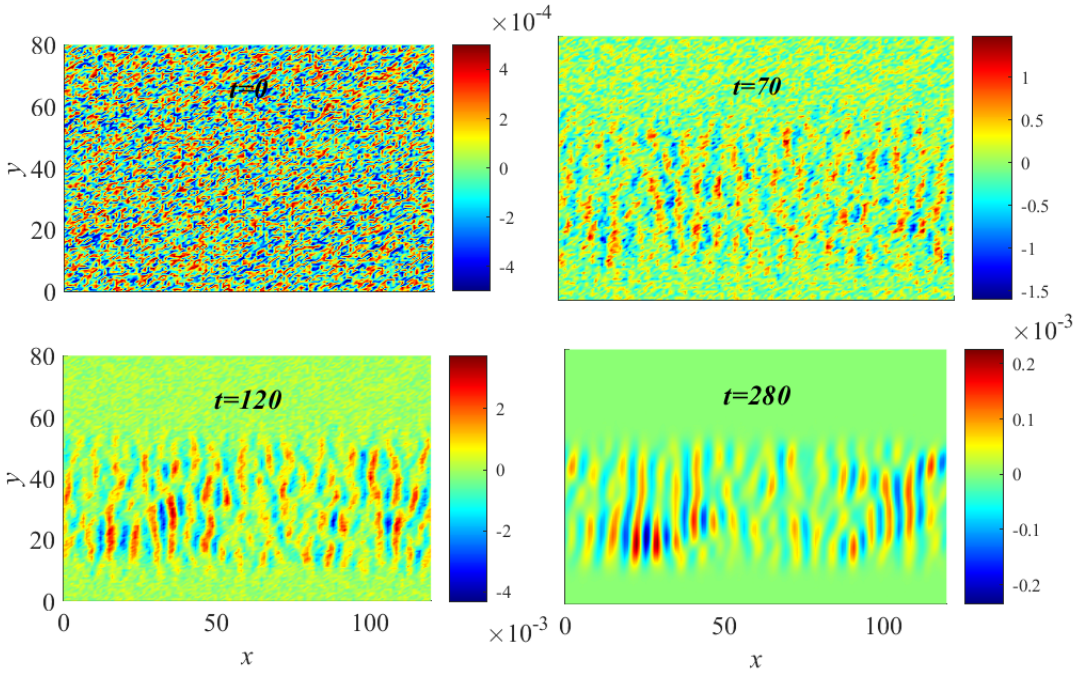

Figure 5.6: Evolution of Φ at different timesteps for $\kappa = 0.25$

5.2.4 *Quantifying the temporal evolution using Statistical Analysis*

5.2.4.1 The Standard Deviation of Φ

The standard deviation $\delta\Phi$ is studied. $\delta\Phi$ peaks over the gradient region. Therefore, there is no spreading of turbulence beyond that region.

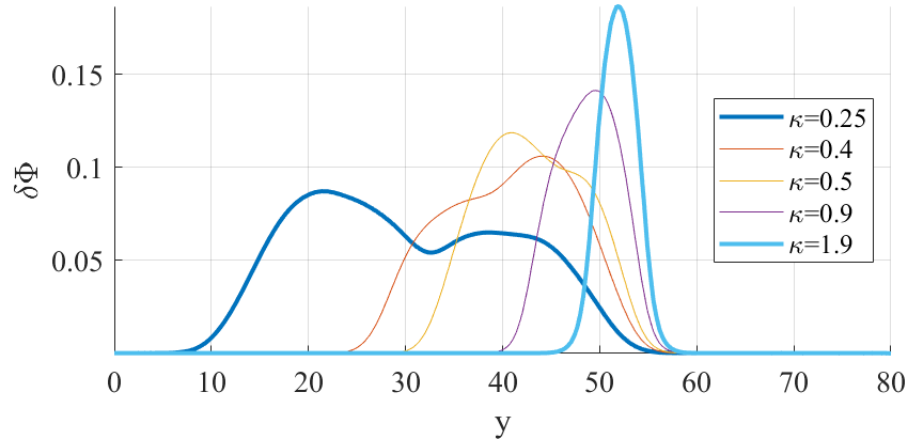

Figure 5.7: Standard deviation of Φ versus y at t_{final}

$\delta\Phi$ increases with time for all values of κ. As κ increases, $\delta\Phi$ increases faster. Evidently, turbulence is linked to K_y, as per our analytical results. The standard deviation of Φ extends over the region of the gradient. There is no spreading of turbulence, as the amplitude growth is only present in the gradient region, which is in agreement with our results on the linear term contribution, and there is no propagation of turbulence into regions without gradients.

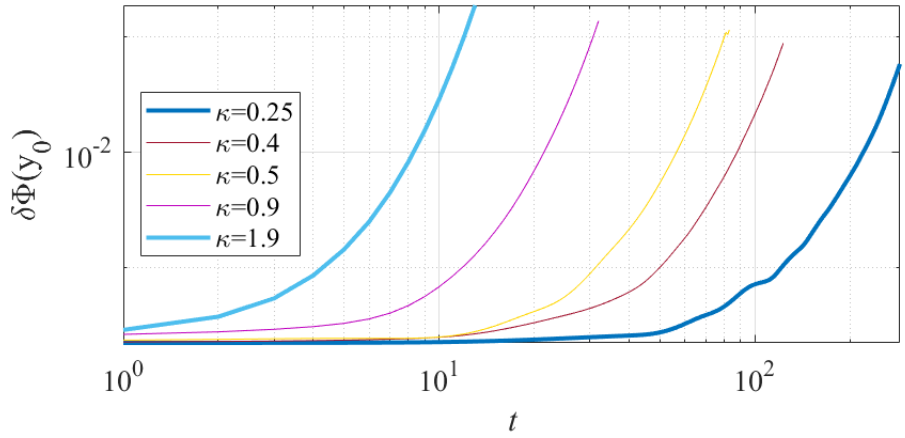

Figure 5.8: Standard deviation of Φ versus time at maximum gradient

5.2.4.2 Studying the k spectrum

The standard deviation shows an increase with time for all values of κ. As the steepness increases, the increase happens over a shorter time. There is no amplitude saturation.

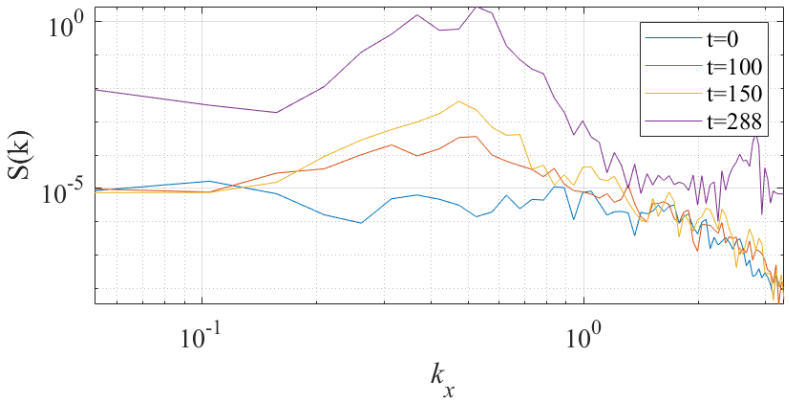

Figure 5.9: Power Spectrum $S(k)$ as a function of k for $\kappa = 0.25$ at different timesteps

The power spectrum gives the energy as a function of scales. It forms a peak around a specific scale, namely k_0, as time increases. The power spectra versus the wavenumbers in the x direction k_x at four different time steps are plotted. As time increases, the power spectra form a peak around a specific scale, named k_0, in other words, k_0 coined the "center of gravity" of the wavenumbers [38], which will be studied in the next section.

5.2.4.3 Studying k_0

k_0 which is $(\int k.S(k)dk)/(\int S(k)d(k))$ where $S(k)$ is the power spectrum and k is the wavenumber is another important parameter to define. The variation of k_0 as a function of y indicates the dominant spatial scales at each position.

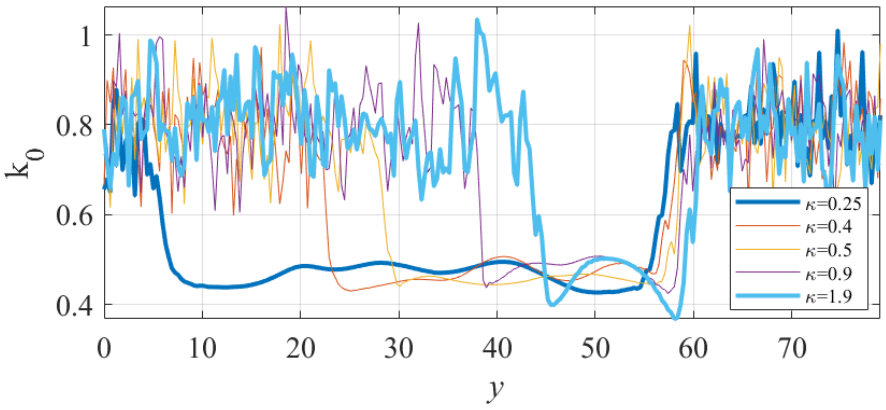

Figure 5.10: k_0 versus y at t_{final}

k_0 at the position of maximum gradient y_0 demonstrates a decrease with time. The larger κ is, the faster the decrease of $k_0(y_0)$ as a function of time.

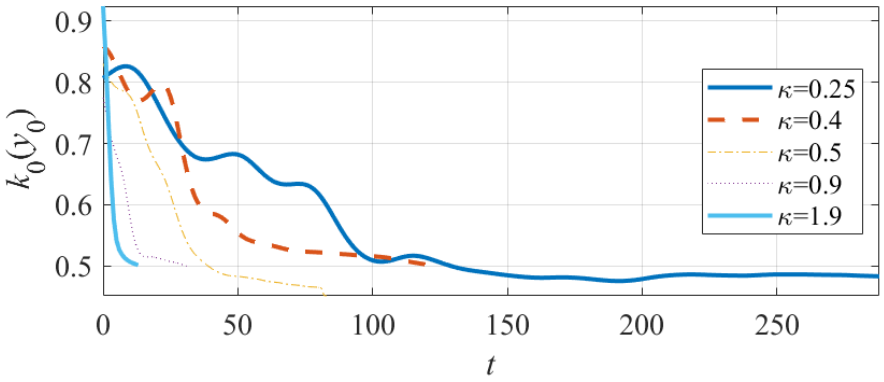

Figure 5.11: k_0 versus time at maximum gradient

At the maximum gradient region, k_0 decreases with time, reaching saturation. This is particularly interesting, because despite amplitude growth, and regardless of the variation in steepness, the spatial structures saturate at a certain wavenumber.

5.3 Cylindrical Hyperbolic Tangent n_0

5.3.1 *White Noise Initial Condition for* Φ

Another type of mesh is the circular mesh. The same initial condition of Φ is used, however a new form of n_0 is used which is $n_0 = \tanh(\kappa(R+a)) - \tanh(\kappa(R-a))$ where $R = \sqrt{(x^2+y^2)}$. The case where $\kappa = 0.4$ and $a = 10$ is studied. The mesh points are taken to be $512 * 512$, resulting in a resolution of approximately $0.7\rho_s$.

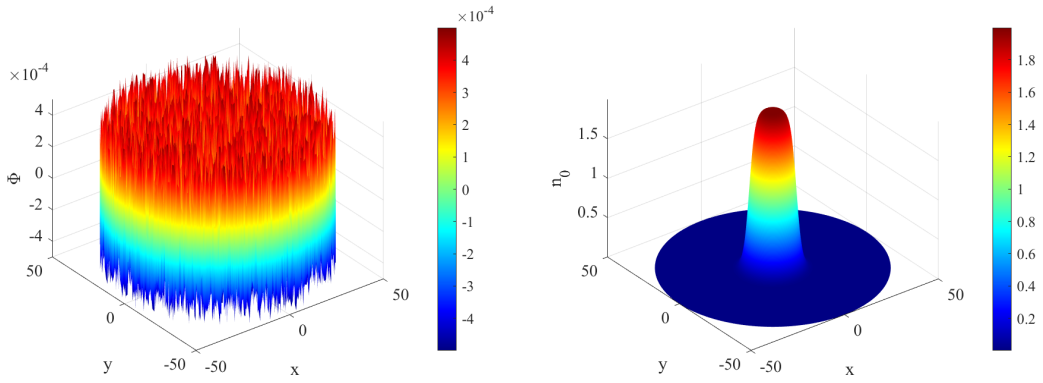

Figure 5.12: The initial conditions of Φ and n_0 for $a = 10$ and $\kappa = 0.4$

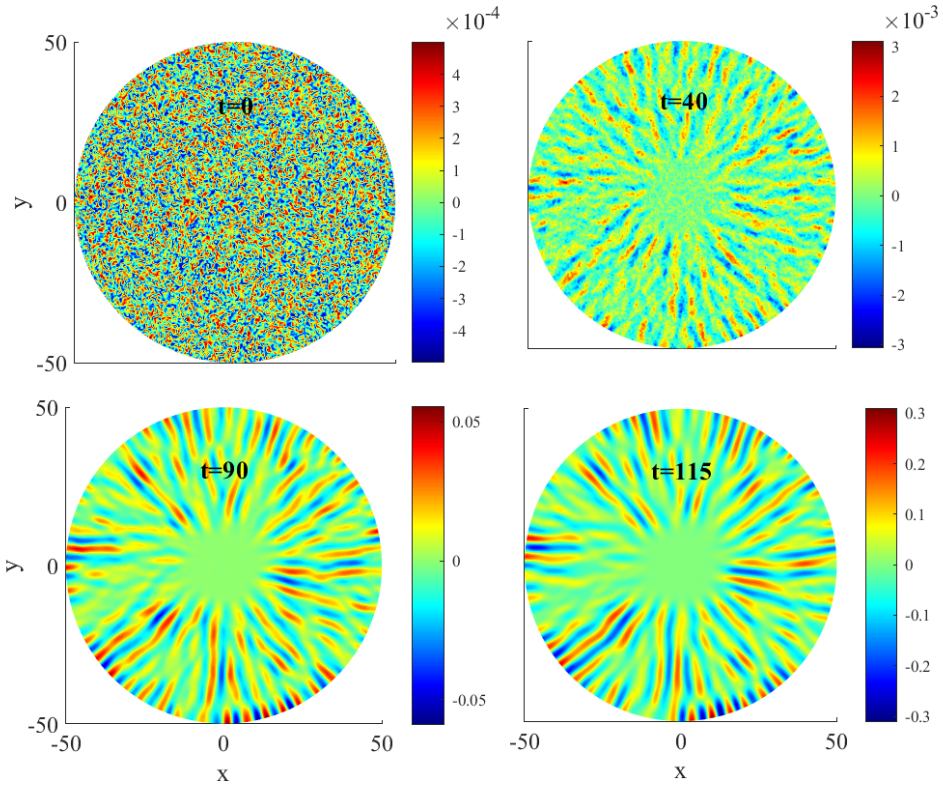

Figure 5.13: Evolution of Φ at different timesteps for $\kappa = 0.4$

An onset of growth in the amplitude of Φ is observed in the gradient region. Rotation in the counterclockwise direction is observed.

5.3.2 *Sine Initial Condition for* Φ

Another case is studied where only the initial form of Φ is changed while n_0 is kept the same. The new form of Φ under study is $\Phi = \Phi_0(\sin(k_1 x) + \sin(k_2 y)$ where $\Phi_0 = 10^{-3}$, and $k_1 = k_2 = 0.2\pi$

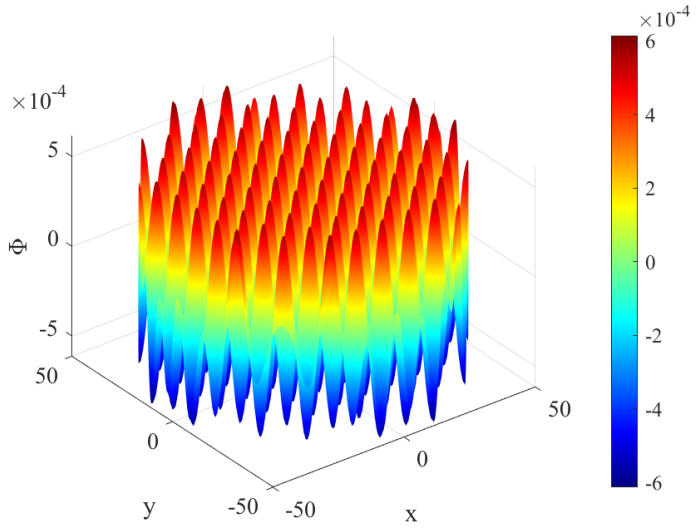

Figure 5.14: The initial condition for a sine wave Φ

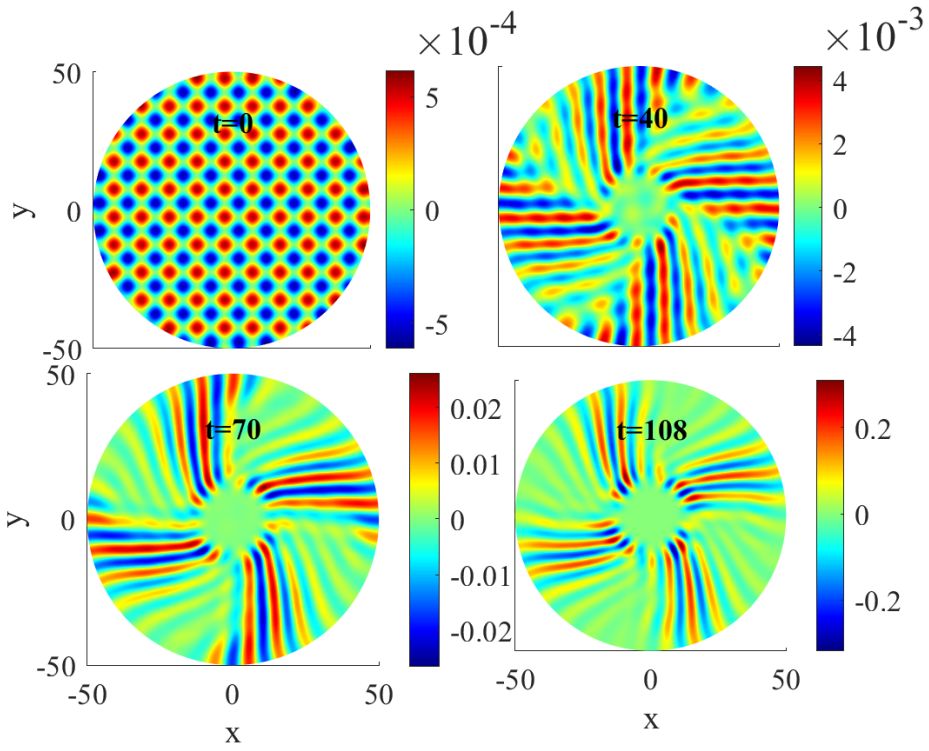

Figure 5.15: Evolution of Φ at different timesteps for $\kappa = 0.4$

Unlike the case of the circular mesh using white noise for the electrostatic potential initial condition, this case shows an onset of double modes in the gradient region. The rotation is also observed to be in the counterclockwise direction.

5.4 Insights and Limitations

Our work on the two-dimensional slab geometry cases shows that there is no spreading of turbulence beyond the gradient region and that despite the increase in amplitude of Φ, the structures reach saturation wavenumber regardless of the density gradient steepness κ. This work, of course, remains incomplete as further analytical investigation is required to determine the factors that affect this saturation wavenumber and its evident independence from the density gradient.

As for the circular mesh case, further work would include observing the power spectra of each simulation, specifically for the case of period doubling observed with the sine initial condition for Φ.

Chapter 6

Conclusion

In this thesis, we have explored the linear and nonlinear dynamics of the Hasegawa-Mima (HM) and Hasegawa-Wakatani (HW) equations, two fundamental models in plasma turbulence studies. In Chapter 3, the HM and HW models were derived from fundamental conservation equations, setting the grounds for further analytical exploration. In chapters 4 and 5, analytical studies of the HM and HW equations were done to find analytical solutions to each model, in addition to the Reynolds number for each equation. Furthermore, the linear HM equation was studied, which provided insights into the role of the linear term on the evolution of the dynamics. Focusing on the dependence of the linear term on the density gradient, the effect of steepness variations on the evolution of electrostatic potential fluctuations was systematically studied. Furthermore, the electrostatic potential is initialized as white noise, and its evolution is studied.

Complementing these analytical studies, in Chapter 6, numerical simulations were performed using FreeFEM++, allowing us to observe the temporal and spatial evolution of electrostatic potential perturbations under the effect of varied density gradient steepness. The numerical results were found to be in agreement with theoretical predictions, reinforcing our understanding of the role of the linear term in electrostatic potential amplitude growth. In addition, statistical analysis of the results was done by computing the standard deviation of Φ as well as power spectra analysis, which emphasized the localization of turbulence and amplitude growth at the maximum gradient region.

Future work can explore the factors determine which wavenumber peaks temporally, as depicted in the power spectrum plots. The numerical study could also be extended by incorporating different forms of the density profile and applying them to a different mesh type to simulate magnetic confinement devices. Specifically in the circular mesh cases, this could be done by modifying the density profile and using better resolutions to get our simulation as close as possible to tokamak simulations.

Appendix A

Single Particle Motion

Before delving into more complex motion to be able to describe plasma behavior, it is first important to analyze how a single particle moves under the effect of magnetic and electric fields. In the case where a particle is not under the effect of any electric or magnetic field -as in an unmagnetized plasma- the particle moves in straight lines unless it undergoes collisions. However, the case is entirely different when a magnetic field is applied. In that case, the particle undergoes a gyration motion. Considering the magnetic field is uniform

$$m\frac{d\vec{v}}{dt} = q(\vec{v} \times \vec{B}) \tag{A.1}$$

Taking the magnetic field to be along the z-direction ($\vec{B} = B\hat{z}$);

$$\begin{aligned} m\dot{v}_x &= q\vec{B}v_y \\ m\dot{v}_y &= -q\vec{B}v_x \\ m\dot{v}_z &= 0 \\ \ddot{v}_x &= \frac{q\vec{B}}{m}\dot{v}_y = -(\frac{q\vec{B}}{m})^2 v_x \\ \ddot{v}_y &= -\frac{q\vec{B}}{m}\dot{v}_x == -(\frac{q\vec{B}}{m})^2 v_y \\ \ddot{v}_z &= 0 \end{aligned} \tag{A.2}$$

This describes a simple harmonic oscillator at the cyclotron frequency, such that the solution to the first and second 2^{nd} order differential equations is the following:

$$\begin{cases} v_y = -v_0 \sin(\omega_c t + \phi), \\ v_x = v_0 \cos(\omega_c t + \phi). \end{cases} \tag{A.3}$$

Where ω_c is the cyclotron frequency:

$$\omega_c = \frac{qB}{m} \tag{A.4}$$

We may choose the phase ϕ so that

$$v_x = v_\perp e^{i\omega ct} = x \tag{A.5}$$

where $v_\perp$ is the speed in the direction perpendicular to $\vec{B}$. Then:

$$v_y = \frac{m}{q\vec{B}} v_x = \pm \frac{1}{\omega_c} \dot{v}_x = \pm i v_\perp e^{i\omega ct} = \dot{y}$$

Integrating once again, we have

$$x - x_0 = i\frac{v_\perp}{\omega_c} e^{i\omega ct} \quad y - y_0 = \pm \frac{v_\perp}{\omega_c} e^{i\omega ct}$$

We define the Larmor radius to be

$$r_L \equiv \frac{v_\perp}{\omega_c} = \frac{m v_\perp}{|q|B}$$

Appendix B

The Hasegawa-Wakatani Model

B.1 Literature on the Hasegawa-Wakatani Model

Ref. [39] aims to derive a model (the Hasegawa-Wakatani model) for describing drift-wave instability near the edge of a tokamak plasma. Then, the results of the numerical solution to this model are shown. To derive this new model, the same assumptions are used as in the derivation of the Hasegawa-Mima model, but the electron-ion collision term is taken into account.

The resultant system of equations shows that the non-linear behavior of resistive drift waves is completely characterized by three parameters $k\rho_s$ where k is defined as $k = |\partial lnn_0/\partial x|$ which is a measure of the density gradient, and $\rho_s = (T_e/m_i)^{1/2}/\omega_{ci}$ which is the ion Larmor radius at the electron temperature T_e, m_i is the ion mass, and ω_{ci} is the ion cyclotron frequency, and c_2 which is the normalized ion viscosity and is equal to $3/10(T_i/T_e)(\nu_{ii}/\omega_{ci})$ where ν_{ii} is the ion-ion collision rate.

B.1.1 *Hasegawa-Wakatani Models in Simulation*

Other papers, such as Ref. [40] aimed to study the stabilization of drift wave fluctuations. This study introduces a novel reduced-order model (ROM)-based feedback control approach for the Modified Hasegawa-Wakatani (MHW) model. ROMs are simplified mathematical representations of complex systems that encapsulate essential system or plasma dynamics, for this case, while reducing computational complexity. The paper proposes a novel approach that combines ROMs with feedback control for the MHW model.

The nonlinear MHW equations are simulated so that the fluctuations can be examined and later stabilized. The results show that as time evolves, both ion vorticity and density fluctuations transition from a horizontally uniform state, the drift wave, to an almost vertically uniform state, namely a zonal flow. A feedback

controller is then utilized to ensure a linear evolution of the density fluctuation.

B.1.2 *Hasegawa-Wakatani on Understanding Turbulence*

Other studies focus on turbulence by examining the nonadiabatic electron response within the framework of the Hasegawa-Wakatani equations, as explored in Ref. [41]. The HW equations offer a simplified model of plasma dynamics, emphasizing the interaction between density and temperature fluctuations in the presence of magnetic fields. These equations are widely applied to investigate the onset and progression of turbulence in magnetized plasmas, with implications for both laboratory fusion experiments and astrophysical systems.

In the adiabatic limit, electrons are assumed to respond instantaneously to variations in the magnetic field, disregarding any time-dependent effects in their motion. By first considering the parallel electron momentum balance equation—while neglecting collisions and electron inertia—a balance emerges between the Lorentz and pressure forces. However, any disruption to this equilibrium requires the electron density and electrostatic potential to adjust accordingly. For example, if an electron density peak forms, the pressure force becomes unbalanced, prompting electrons to flow outward, which in turn lowers the density in that region. As a result, ions also undergo polarization drift away from the peak, necessitating an increase in the electrostatic potential. This self-regulating process leads to a decrease in electron density and a corresponding rise in the electrostatic potential to restore force balance.

This study derives a near-adiabatic one-field reduction of the HW equations, which conceptually represents fast parallel electron motion compared to the slower parallel ion motion relative to the characteristic frequencies of perpendicular drifts. This reduction is achieved by decomposing the electrostatic potential into its adiabatic and nonadiabatic components.

B.1.3 *Hasegawa-Wakatani Solutions*

Ref. [42] examines the linearized HW equations, specifically in the limit where resistivity approaches zero. The study demonstrates the existence and uniqueness of a solution over a certain time interval for the initial value problems associated with the HW equations. Additionally, it establishes that the solution of the HW equations converges to that of the drift wave turbulence model equations in the zero-resistivity limit.

Ref. [43] investigates the existence of unique global-in-time solutions for the HW equations. The study first considers the HW equations in a cylindrical domain with almost-periodic initial conditions along the z-direction and establishes the existence and uniqueness of a solution for this system. Additionally, it proves that

the solution converges in the zero-resistivity limit.

The paper also explores the behavior of the HW equations under different limits of the adiabaticity parameter α. It concludes that asα approaches zero, the first HW equation reduces to the two-dimensional incompressible Navier-Stokes equation for $\nabla_\perp \Phi$. Conversely, when α tends to infinity, the HW equations transform into the Hasegawa-Mima (HM) equation. Notably, the limit $\alpha \to \infty$ is shown to be equivalent to the resistivity η approaching zero.

B.1.4 *Hasegawa-Wakatani Stability Analysis*

Ref. [44] examines the transition between turbulence-dominated and zonal flow-dominated regimes using the Hasegawa-Wakatani model. Through linear stability analysis, it is shown that a bifurcation in the HW equations marks the onset of drift wave turbulence, the formation of zonal flows, and their eventual destabilization, leading to renewed turbulence. The analysis begins with a modified HW system that excludes zonal components, allowing for the derivation of an equation governing their evolution.

Stability is determined by a threshold involving parameters such as the dissipation coefficient D, the adiabaticity parameter α, and the density gradient. When this threshold is exceeded, turbulence grows until nonlinear effects dominate. The study also finds two distinct saturated states: a zonal flow-dominated regime where turbulence is suppressed and an isotropic turbulence-dominated regime. Zonal flows are prevalent in the adiabatic limit ($\alpha \gg 1$), while isotropic turbulence dominates when $\alpha \ll 1$. Finally, zonal flow stability is analyzed using an eigenvalue equation, which, in the adiabatic limit, reduces to the Rayleigh equation for neutral fluids.

B.2 The Hasegawa-Wakatani Model

Similar to the HM model, the Hasegawa-Wakatani [39] model is often applied to study turbulence and transport in the edge regions of tokamaks, where the plasma interacts with material surfaces. This is crucial for optimizing plasma performance, preventing damage to the plasma-facing components, and ensuring the success of fusion reactions. One of the most important assumptions when deriving the HM model is ignoring the collisions, which leads to obtaining an adiabatic response of electrons. We use the same assumptions for the Hasegawa-Wakatani model as we did for the Hasegawa-Mima model, except that electron-ion collisions and ion viscosity are kept. The Hasegawa-Wakatani model serves the same purpose as the Hasegawa-Mima Model, but it incorporates the effects of collisions and viscosity to understand turbulence. The assumptions that this model uses are as follows

1. Magnetic field is uniform and along z-direction $\vec{B} = B_0\hat{z}$
2. Inhomogeneous plasma along y-direction $n_0 = n_0(y)$
3. Cold ions: $T_i \ll T_e \Rightarrow p_i = nT_i = 0$
4. Equations of motion $\perp \vec{B}$.
5. Because $\frac{m_e}{m_i} \ll 1 \rightarrow \vec{u}_{e\|} \gg \vec{u}_{i\|}$ in the parallel direction, so ions are assumed to be immobile: $\vec{u}_{i\|} = 0$. So, the dynamics in the parallel direction are governed by the elections alone
6. Keeping Collisions

To derive the HW model, a similar approach as was used to derive the HM model is applied. The derivation begins from fundamental conservation equations, namely the continuity equations and the momentum balance equations.

B.2.1 *Electron Continuity*

$\frac{\partial n_e}{\partial t} + \vec{\nabla}_\perp (n_e\vec{u}_e) + \vec{\nabla}_\| (n_e\vec{u}_e) = 0$

In the $\perp$ dynamics, the motion of electrons is dominated by the $\vec{E} \times \vec{B}$ drift and the polarization drift is neglected

$$\begin{aligned}
&\frac{\partial (n_{e0} + \delta n_e)}{\partial t} + \vec{\nabla}_\perp \left((n_{e_0} + \delta n_e)\, \vec{u}_E \right) + \vec{\nabla}_\| \left((n_{e0} + \delta n_e)\, \vec{u}_{e\|} \right) = 0 \\
&\left(\frac{\partial}{\partial t}\delta n_e + \vec{\nabla}_\perp (\delta n_e \vec{u}_E) + \vec{\nabla}_\| \left(n_{e0}\vec{u}_{e\|} \right) = 0 \right) \div n_{e0} \\
&\frac{\partial}{\partial t}\left(\frac{\delta n_e}{n_{e0}} \right) + \vec{u}_E \vec{\nabla}_\perp \left(\frac{\delta n_e}{n_{e0}} \right) + \frac{\delta n_e}{n_{e0}} \vec{\nabla}_\perp \vec{u}_e \\
&\left(\frac{\partial}{\partial t} + \vec{u}_E \vec{\nabla}_\perp \right) \left(\frac{\delta n_e}{n_{e0}} + \ln\left(\frac{n_{e_0}}{\omega_{ci}} \right) \right) + \vec{\nabla}_\| \cdot \vec{u}_{e\|} = 0
\end{aligned} \tag{B.1}$$

To determine $\vec{u}_{e\perp}$, we use the perpendicular momentum balance equation for electrons, and to determine $\vec{u}_{e||}$, we use the parallel momentum balance equation for electrons

B.2.2 *Parallel Electron Momentum Balance Equation*

$$m_e n_e \left[\frac{\partial \vec{u}_e}{\partial t} + \left(\vec{u}_e \cdot \vec{\nabla} \right) \cdot \vec{u}_e \right] = \vec{\nabla} p + \vec{F}_{\text{Lorentz}} + \vec{F}_{\text{collisions}}$$

$$\vec{u}_{i\parallel} = 0$$

So the parallel momentum balance equation becomes:

$$\begin{aligned} \overrightarrow{0} &= -T_e\vec{\nabla}_\parallel n_e + n_e e\vec{\nabla}_\parallel\Phi - \eta e^2 n^2 \vec{u}_{e\parallel} \\ \vec{F}_{e\parallel} &= -m_e n_e \nu_{ei}\vec{u}_{e\parallel} = -\eta^2 e^2 n^2 \vec{u}_{e\parallel} \end{aligned} \tag{B.2}$$

Where η is the plasma resistivity:$\eta = \frac{m_e\nu_{ei}}{ne^2}$

We neglect the viscosity of electrons because of their small mass but keep the collision term and define the current Density:

$$\begin{aligned} \vec{J} &= ne\left(\vec{u}_i - \vec{u}_e\right) \\ \vec{u}_{i\parallel} &= 0 \\ \vec{J}_\parallel &= -ne\vec{u}_{e\parallel} \end{aligned} \tag{B.3}$$

Adding a first-order perturbation to density and electrostatic potential such that $n_e = n_{e_0} + \delta n_e$ and $\Phi = 0 + \Phi$

$$\begin{aligned} \vec{0} &= -T_e\vec{\nabla}_\parallel\left(n_{e0} + \delta n_e\right) - \left(n_{e0} + \delta n_e\right)e\vec{\nabla}_\parallel\Phi + \eta e(n_{e0} + \delta n_e)\vec{J}_\parallel \\ \eta e n_{e0}\vec{J}_\parallel &= T_e\vec{\nabla}_\parallel\left(\delta n_e + \delta n_{e0}\right) - \left(n_{e0} + \delta n_e\right)e\vec{\nabla}_\parallel\Phi \\ \eta e n_{e0}\vec{J}_\parallel &= T_e\vec{\nabla}_\parallel(\delta n_e) - n_{e0}e\vec{\nabla}_\parallel\Phi \\ \vec{J}_\parallel &= \frac{T_e}{\eta e}\vec{\nabla}_\parallel(\frac{\delta n_e}{n_{e0}} - \frac{e\phi}{T_e}) \\ \vec{u}_{e\parallel} &= -\frac{1}{ne}\vec{J}_\parallel = -\frac{T_e}{n\eta e^2}\vec{\nabla}_\parallel\left(\frac{\delta n_e}{n_{e0}} - \frac{e\Phi}{T_e}\right) \end{aligned} \tag{B.4}$$

So, we have obtained the parallel electron velocity, what remains is obtaining the perpendicular electron velocity.

B.2.3 *Perpendicular Momentum Balance Equation for Electrons*

$$\begin{aligned} &\left(\vec{0} = -\vec{\nabla}_\perp p_e - n_e e\left(-\vec{\nabla}_\perp\Phi + \vec{u}_{e\perp}\times\vec{B}\right)\right)\times\vec{B} \\ &\vec{0} = -\vec{\nabla}_\perp p_e\times\vec{B} - n_e\left(-\vec{\nabla}_\perp\Phi\times\vec{B} + \left(\vec{u}_{e\perp}\times\vec{B}\right)\times\vec{B}\right) \\ &\vec{0} = -\vec{\nabla}_\perp p_e\times\vec{B} + n_e e\vec{\nabla}_\perp\Phi\times\vec{B} - ne\left(\vec{u}_{e\perp}\times\vec{B}\right)\times\vec{B} \\ &n_e e\left(\overrightarrow{u_{e\perp}}\times\vec{B}\right)\times\vec{B} = -\vec{\nabla}_\perp p_e\times\vec{B} + ne\vec{\nabla}_\perp\Phi\times\vec{B} \\ &\left(\vec{u}_{e\perp}\times\vec{B}\right)\times\vec{B} = -\frac{1}{n_e}\vec{\nabla}_\perp\left(n_e T_e\right)\times\vec{B} + \vec{\nabla}_\perp\Phi\times\vec{B} \\ &\left(\vec{u}_{e\perp}\times\vec{B}\right)\times\vec{B} = \frac{-T_e}{n_e}\vec{\nabla}_\perp n_e\times\vec{B} + \vec{\nabla}_\perp\Phi\times\vec{B} \end{aligned} \tag{B.5}$$

$$\Rightarrow \vec{u}_{e\perp} = -\frac{\vec{\nabla}_\perp \Phi \times \vec{B}}{B^2} + \frac{T}{n_e B^2}\vec{\nabla}_\perp n_e \times \vec{B} \tag{B.6}$$

The polarization drift is neglected for electrons because of their small mass, while the diamagnetic drift is neglected for ions because of the assumption of cold ions.

Plugging in $\vec{u}_{e\parallel}$ and $\vec{u}_{e\perp}$ into the electron continuity equation

$$\left(\frac{\partial}{\partial t} + \vec{u}_E \vec{\nabla}_\perp\right)\left(\frac{\delta n_e}{n_{e0}} + \ln\left(\frac{n_{e_0}}{\omega_{ci}}\right)\right) + \vec{\nabla}_\parallel \cdot \vec{u}_{e\parallel} = 0 \tag{B.7}$$

So the 1st Hasegawa-Wakatani equation is:

$$\left(\frac{\partial}{\partial t} + \vec{u}_e \vec{\nabla}_\perp\right)\left(\frac{\delta n_e}{n_{e0}} + \ln\left(\frac{n_{e0}}{\omega_{ci}}\right)\right) + \frac{T_e}{\eta e^2 n_{e0}}\vec{\nabla}_\parallel^2\left(\frac{e\Phi}{T_e} - \frac{\delta n_e}{n_{e0}}\right) = 0 \tag{B.8}$$

B.2.4 *Ion Continuity Equation*

$$\begin{aligned}
&\vec{u}_i = \vec{u}_E + \vec{u}_p + \vec{u}_{\text{visc}} \\
&\partial_t n_i + \vec{\nabla}(n_i \vec{u}_i) = 0 \\
&\left(\partial_t n_i + n_i \vec{\nabla}\cdot\vec{u}_i + \vec{u}_i \cdot \vec{\nabla} n_i\right) \div n_i \\
&\frac{\partial_t n_i}{n_i} + \vec{\nabla}\cdot\vec{u}_i + \frac{\vec{u}_i \cdot \vec{\nabla} n_i}{n_i} = 0
\end{aligned} \tag{B.9}$$

Therefore,

$$\begin{aligned}
&\frac{d}{dt}\ln\left(\frac{n_i}{\omega_{ci}}\right) + \vec{\nabla}_\perp \vec{u}_i = 0 \\
&\vec{\nabla}\cdot\vec{u}_i = \vec{\nabla}\cdot\vec{u}_E + \vec{\nabla}\cdot\vec{u}_p + \vec{\nabla}\cdot\vec{u}_{\text{visc}}
\end{aligned} \tag{B.10}$$

We'll name the zeroth, first, and second-order terms of the perpendicular ion velocity $\vec{u}_E$, $\vec{u}_p$, and $\vec{u}_{visc}$, respectively.

First, we linearize the perpendicular momentum balance equation for ions to the zeroth order:

$$\begin{aligned}
&\vec{0} = -n_i e(\vec{\nabla}_\perp \Phi + \vec{u}_{E\perp} \times \vec{B}_\perp) \\
&\vec{0} = -n_i e(\vec{\nabla}_\perp \Phi \times \vec{B} + (\vec{u}_{E\perp} \times \vec{B}_\perp) \times \vec{B}) \\
&-\vec{\nabla}_\perp \Phi \times \vec{B} = (\vec{u}_{E\perp} \times \vec{B}_\perp) \times \vec{B} \\
&-\vec{\nabla}_\perp \Phi \times \vec{B} = (\vec{u}_{E\perp} \cdot \vec{B})\vec{B}_\perp - (\vec{B}_\perp \cdot \vec{B})\vec{u}_{E\perp} \\
&\text{Therefore, } \vec{u}_E = \frac{-\vec{\nabla}_\perp \Phi \times \vec{B}}{B^2}
\end{aligned} \tag{B.11}$$

Linearizing to the first-order:

$$\begin{aligned}
&\frac{d\vec{u}_i}{dt} = \frac{e}{m_i}\vec{E}_\perp + \frac{e}{m_i}\vec{u}_E \times \vec{B} + \frac{e}{m_i}\vec{u}_p \times \vec{B} \\
&\text{But,} \vec{0} = \frac{e}{m_i}\vec{E}_\perp + \frac{e}{m_i}\vec{u}_E \times \vec{B} \\
&\text{So,} \frac{d\vec{u}_E}{dt} = \frac{e}{m_i}\vec{u}_p \times \vec{B} \\
&\vec{u}_p = \frac{1}{\omega_{ci}B}\frac{d\vec{E}_\perp}{dt} = \frac{-1}{\omega_{ci}}\frac{d\vec{\nabla}_\perp\Phi}{dt}
\end{aligned} \tag{B.12}$$

We then follow the same procedure and linearize to the second order to obtain the expression of the viscosity drift.

$$\vec{u}_{viscosity} = \frac{\mu}{\omega_{ci}B}\vec{\nabla}^3_\perp\Phi \tag{B.13}$$

Plugging back into the continuity equation:

$$d_t ln(\frac{n_i}{\omega_{ci}}) + \frac{\mu}{\omega_{ci}B}\vec{\nabla}^4_\perp\Phi - \frac{1}{\omega_{ci}B}\frac{d\vec{\nabla}^2_\perp\Phi}{dt} = 0 \tag{B.14}$$

So, we obtain the second Hasegawa-Wakatani equation:

$$\frac{d(ln(\frac{n_i 0}{\omega_{ci}}) + \frac{\delta n_i}{n_{i0}} - \frac{1}{\omega_{ci}B}\vec{\nabla}^2_\perp\Phi)}{dt} + \frac{\mu}{\omega_{ci}B}\vec{\nabla}^4_\perp\Phi = 0 \tag{B.15}$$

To normalize the Hasegawa-Wakatani equations, we use the following conversions: $\omega_{ci}t \rightarrow t$, $\frac{x,y}{\rho_s} \rightarrow x, y$, $\frac{e\Phi}{T} \rightarrow \Phi$ where $\rho_s = \sqrt{\frac{T_e}{m_i}}\frac{1}{\omega_{ci}}$, and $\delta n/n_0 \rightarrow n$.

$$\begin{aligned}
(\frac{\partial}{\partial t} - (\vec{\nabla}_\perp\Phi \times \hat{z}) \cdot \vec{\nabla}_\perp)\vec{\nabla}^2_\perp\Phi = \alpha(\Phi - n) + D\vec{\nabla}^4_\perp\Phi \\
(\frac{\partial}{\partial t} - (\vec{\nabla}_\perp\Phi \times \hat{z}))(n + ln(\frac{n_0}{\omega_{ci}})) = \alpha(\Phi - n)
\end{aligned} \tag{B.16}$$

where $\alpha = -\frac{T}{e^2 n_0 \eta \omega_{ci}}\vec{\nabla}^2_{||}$ and $D = \frac{\mu}{\rho_s^2 \omega_{ci}}$

B.3 Analytical Approaches to the HW Model

The normalized Hasegawa-Wakatani equations are

$$\begin{aligned}
(\frac{\partial}{\partial t} - (\vec{\nabla}_\perp\Phi \times \hat{z}) \cdot \vec{\nabla}_\perp)\vec{\nabla}^2_\perp\Phi = \alpha(\Phi - n) + D\vec{\nabla}^4_\perp\Phi \\
(\frac{\partial}{\partial t} - (\vec{\nabla}_\perp\Phi \times \hat{z}))(n + ln(\frac{n_0}{\omega_{ci}})) = \alpha(\Phi - n)
\end{aligned} \tag{B.17}$$

where $\alpha = -\frac{T_e}{e^2 n_0 \eta \omega_{ci}} \vec{\nabla}_{||}^2$ and $D = \frac{\mu}{\rho_s^2 \omega_{ci}}$

It is important to note that $\alpha(\Phi - n)$ is the term representing adiabaticity, which is a measure of the electron adiabatic response along the magnetic field lines [45]. It also controls the strength of the resistive coupling between n and Φ. In the limit $\alpha \gg 1$, the coupling is adiabatic, which means that the density and potential perturbations are in phase. Since α controls the phase difference between Φ and n, then it controls the transport as well [46] by controlling how fast the electrostatic potential reacts to perturbation in the density. When $\alpha \gg 1$, the reaction is instantaneous [47]. In this case, the HW equations reduce to the HM equation [48]. α is of the order of 1 [49].

D is the dissipation term, which is essentially a viscosity parameter and is usually estimated to be of the order of 10^{-3}. However, it can also be expressed as $D = \frac{3}{10}(T_i/T_e)(\nu_i i/\omega_{ci})$, so following from the HW model assumption of $T_i = 0$, $D \approx 0$, which is the case for most plasmas [39].

Using Poisson brackets, the Hasegawa-Wakatani equations can be expressed as

$$\begin{aligned} \frac{\partial}{\partial t}(\vec{\nabla}_\perp^2 \Phi) &= \alpha(\Phi - n) + \{\vec{\nabla}_\perp^2 \Phi, \Phi\} + D\vec{\nabla}_\perp^4 \Phi \\ \frac{\partial n}{\partial t} &= \alpha(\Phi - n) + \{ln(\frac{n_0}{\omega_{ci}}), \Phi\} + \{n, \Phi\} \end{aligned} \tag{B.18}$$

Transforming to Fourier modes such that $n = \bar{n} e^{i(k_x x + k_y y - i\omega t)}$ and $\Phi = \bar{\Phi} e^{i(k_x x + k_y y - i\omega t)}$. The nonlinear term in the first HW equation is $\{\vec{\nabla}_\perp^2 \Phi, \Phi\}$, and in the second HW equation it is $\{n, \Phi\}$. Therefore, to find the effective Reynolds number, we follow the same procedure as for the HM model. The effective Reynolds number for the first Hasegawa-Wakatani equation can be obtained as follows, assuming that $k_x = k_y$

$$\begin{aligned} R_\Phi &= \frac{\{\vec{\nabla}_\perp^2 \Phi, \Phi\}}{D\vec{\nabla}_\perp^4 \Phi} \\ R_\Phi &= \frac{k_x k_y k_\perp^2 \Phi^2}{D k_\perp^4 \Phi} \approx \frac{\Phi}{D} \end{aligned} \tag{B.19}$$

Therefore, when $R_\Phi \ll 1$, $\Phi \ll D$, which means that the dissipation is greater than the electrostatic potential, it suggests that the nonlinear effects dominate over dissipation. Otherwise, if $R_\Phi \gg 1$, $\Phi \gg D$, the electrostatic potential is greater than the dissipation term, it indicates that dissipation is relatively stronger compared to nonlinear effects. In this case, the system may exhibit more damping, and the influence of nonlinear interactions might be suppressed.

To find an estimate of the value of R_Φ, consider $\Phi \approx 10^{-3}$, and $D = \mu/\rho_s^2 \omega_{ci} \approx 10^{-3}$, so $R_\Phi = 1$.

As for the second Hasegawa-Wakatani equation, the effective Reynolds number R_n is as follows

$$\begin{aligned} R_n &= \frac{\{n, \Phi\}}{\{ln(\frac{n_0}{\omega_{ci}}), \Phi\}} \\ R_n &= \frac{k_x k_y n \Phi}{k_y \Phi / L_n} = L_n k n \end{aligned} \tag{B.20}$$

When $R_n \ll 1$, $L_n k n \ll 1$, in this case, the linear term dominates; on the other hand, when $R_n \gg 1$, $L_n k n \gg 1$, in which case the nonlinear term dominates. Setting $L_n \approx 100$, $k \approx 10$, and $n = \delta n / n_0 \approx 10^{-2}$, we obtain $R = 10$.

B.3.1 *HW Dispersion Relation*

B.3.1.1 Solving the HW Equations Analytically

$$\begin{aligned} (\frac{\partial}{\partial t} - (\vec{\nabla}_\perp \Phi \times \hat{z}) \cdot \vec{\nabla}_\perp) \vec{\nabla}_\perp^2 \Phi &= \alpha(\Phi - n) + D \vec{\nabla}_\perp^4 \Phi \\ (\frac{\partial}{\partial t} - (\vec{\nabla}_\perp \Phi \times \hat{z}))(n + ln(\frac{n_0}{\omega_{ci}})) &= \alpha(\Phi - n) \end{aligned} \tag{B.21}$$

Isolating the time derivatives of Φ and n on the left-hand side

$$\begin{aligned} \frac{\partial}{\partial t}(\vec{\nabla}_\perp^2 \Phi) &= \alpha(\Phi - n) + D \vec{\nabla}_\perp^4 \Phi \\ \frac{\partial n}{\partial t} &= \alpha(\Phi - n) - i \Phi k_\perp (\hat{z} \times \vec{\nabla}_\perp ln(\frac{n_0}{\omega_{ci}})) \end{aligned} \tag{B.22}$$

B.3.1.1.1 Initial Conditions on Φ and n First, we consider the case where $\Phi = 0$, and $n = 0$; it is immediately evident that there is no condition on the $\vec{\nabla} n$ for the system of equations to be valid.

B.3.1.1.2 Steady State In the steady state, the above system of equations becomes

$$\begin{aligned} \alpha(\Phi - n) &= D \vec{\nabla}_\perp^4 \Phi \\ \alpha(\Phi - n) &= \frac{\partial \Phi}{\partial x} \frac{1}{L_n} \end{aligned} \tag{B.23}$$

Equating the right-hand side of the two equations, we obtain

$$D \vec{\nabla}_\perp^4 \Phi = \frac{\partial \Phi}{\partial x} \frac{1}{L_n} \tag{B.24}$$

We consider Φ to be one-dimensional of the form $\Phi = \bar{\Phi}e^{-ik_x x}$ or $\Phi = \bar{\Phi}\cos k_x x$. Therefore, the equation becomes

$$\begin{aligned} Dk_x^4\Phi &= -ik_x\Phi\frac{1}{L_n} \\ Dk_x^4\Phi &= \tan k_x x\frac{1}{L_n} \end{aligned} \tag{B.25}$$

Hence

$$k_x^4 = \frac{1}{L_n}\frac{1}{D}\tan k_x x \tag{B.26}$$

This sets conditions on k_x, L_n, and D such that the forms of Φ and n are steady-state solutions.

B.3.1.1.3 Non-Steady State/Time Variation The linear non-steady state HW equations in one dimension are

$$\begin{aligned} \frac{\partial}{\partial t}(\frac{\partial^2}{\partial x^2}\Phi) &= \alpha(\Phi - n) + D\frac{\partial^4}{\partial x^4}\Phi \\ \frac{\partial n}{\partial t} &= \alpha(\Phi - n) + \frac{\partial}{\partial y}ln(n_0)\frac{\partial}{\partial x}\Phi \end{aligned} \tag{B.27}$$

We consider Φ and n of the form $\Phi = \Phi_0(t)\cos(k_x x)$ and $n = n_0(t)\cos(k_x x)$, so the equations become

$$\begin{aligned} -k_x^2\frac{\partial\Phi_0(t)}{\partial t}\cos(k_x x) &= \alpha(\Phi - n) + Dk_x^4\Phi \\ \frac{\partial n_0(t)}{\partial t}\cos(k_x x) &= \alpha(\Phi - n) - \frac{1}{L_n}k_x\Phi_0\sin(k_x x) \end{aligned} \tag{B.28}$$

Setting $\alpha(\Phi - n) = \alpha(\Phi - n)$,

$$-k_x^2\frac{\partial\Phi_0(t)}{\partial t}\cos(k_x x) - Dk_x^4\Phi_0\cos(k_x x) = \frac{\partial n_0(t)}{\partial t}\cos(k_x x) + \frac{1}{L_n}k_x\Phi_0\sin(k_x x) \tag{B.29}$$

Simplifying the equation

$$\frac{1}{k_x^2}\frac{\partial n_0(t)}{\partial t} + \frac{\Phi_0(t)}{\partial t} = (-\frac{1}{L_n k_x}\tan(k_x x) - Dk_x^2)\Phi_0(t) \tag{B.30}$$

B.3.1.2 Solving the HW Equations using Fourier modes

Taking the case where $R \ll 1$, our equations become linear such that

$$\begin{aligned} i\omega k_\perp^2\Phi &= \alpha(\Phi - n) + Dk_\perp^4\Phi \\ -i\omega n &= \alpha(\Phi - n) - i\Phi\vec{k}_\perp \cdot (\hat{z} \times \vec{\nabla}_\perp ln(\frac{n_0}{\omega_{ci}})) \end{aligned} \tag{B.31}$$

Rearranging the equations

$$\begin{aligned} i\omega k_\perp^2 - \alpha - Dk_\perp^4\phi_k + \alpha n_k = 0 \\ ik_\perp \cdot (\hat{z} \times \nabla_\perp \ln\left(\frac{n_0}{\omega_{ci}}\right)) - \alpha\phi_k + (\alpha - i\omega)n_k = 0 \end{aligned} \tag{B.32}$$

Solving this system of equations, we obtain the following dispersion relation

$$\omega^2 + i\omega\left[\alpha\left(1 + \frac{1}{k_\perp^2}\right) + Dk_\perp^2\right] - \alpha Dk_\perp^2 - i\alpha\vec{k}_\perp \cdot (\hat{z} \times \vec{\nabla}_\perp \ln\left(\frac{n_0}{\omega_{ci}}\right))k_\perp^2 = 0 \tag{B.33}$$

If we take the limit of no dissipation ($D = 0$), we obtain

$$\omega^2 + i\omega\alpha\left(1 + \frac{1}{k_\perp^2}\right) - i\alpha\vec{k}_\perp \cdot (\hat{z} \times \vec{\nabla}_\perp \ln\left(\frac{n_0}{\omega_{ci}}\right))k_\perp^2 = 0 \tag{B.34}$$

Setting $\alpha \to \infty$, the dispersion relation becomes

$$\omega = \frac{(\hat{z} \times \nabla_\perp \ln(\frac{n_0}{\omega_{ci}})) \cdot \mathbf{k}_\perp}{k_\perp^2 + 1} \tag{B.35}$$

Bibliography

[1] H. Karakazian, S. Moufawad, and N. Nassif, "A finite-element model for the hasegawa–mima wave equation," *Applied Mathematics and Computation*, vol. 412, p. 126 550, 2022.

[2] R. J. Goldston, *Introduction to plasma physics*. CRC Press, 2020.

[3] W. B. Thompson, *An introduction to plasma physics*. Elsevier, 2013.

[4] F. F. Chen *et al.*, *Introduction to plasma physics and controlled fusion*. Springer, 1984, vol. 1.

[5] A. Rauf and S. Kousar, "Astrophysical plasma physics: Understanding the behavior of matter in extreme environments," *WORLDWIDE JOURNAL OF PHYSICS*, vol. 4, no. 02, pp. 8–15, 2023.

[6] G. K. Parks, *Physics of space plasmas: an introduction*. CRC Press, 2019.

[7] G. Paschmann, S. Haaland, and R. A. Treumann, *Auroral plasma physics*. Springer Science & Business Media, 2003, vol. 15.

[8] D. A. Gurnett and A. Bhattacharjee, *Introduction to plasma physics: with space and laboratory applications*. Cambridge university press, 2005.

[9] A. Hasegawa and K. Mima, "Strong turbulence, self-organization and plasma confinement," *The European Physical Journal H*, vol. 43, pp. 499–521, 2018.

[10] M. Kikuchi, *Frontiers in fusion research: physics and fusion*. Springer Science & Business Media, 2011.

[11] L. Artsimovich, "Tokamak devices," *Nuclear Fusion*, vol. 12, no. 2, p. 215, 1972.

[12] J. J. Chapman, "Advanced fusion reactors for space propulsion and power systems," *2011 Abstracts IEEE International Conference on Plasma Science*, 2011. DOI: 10.1109/plasma.2011.5992998.

[13] C. Yamanaka, "Inertial confinement fusion: The quest for ignition and energy gain using indirect drive," *Nuclear Fusion*, vol. 39, no. 6, pp. 825–827, 1999.

[14] S. Atzeni, A. Schiavi, F. Califano, *et al.*, "Fluid and kinetic simulation of inertial confinement fusion plasmas," *Computer physics communications*, vol. 169, no. 1-3, pp. 153–159, 2005.

[15] J. Wesson and D. J. Campbell, *Tokamaks*. Oxford university press, 2011, vol. 149.

[16] S. E. Hunyadi Murph and M. A. Murph, "Nuclear fusion: The promise of endless energy," *Physical Sciences Reviews*, vol. 8, no. 10, pp. 3095–3118, 2023.

[17] L. Spitzer Jr, "The stellarator concept," *The Physics of Fluids*, vol. 1, no. 4, pp. 253–264, 1958.

[18] W. D. McComb, *The physics of fluid turbulence*. Oxford university press, 1990.

[19] P. M. Bellan, *Fundamentals of plasma physics*. Cambridge university press, 2008.

[20] R. G. Mills, "Lawson criteria," *IEEE Transactions on Nuclear Science*, vol. 18, no. 4, pp. 205–207, 1971.

[21] A. Hasegawa and K. Mima, "Pseudo-three-dimensional turbulence in magnetized nonuniform plasma," *The Physics of Fluids*, vol. 21, no. 1, pp. 87–92, 1978.

[22] J. G. Charney, "On the scale of atmospheric motions," in *The Atmosphere—A Challenge: The Science of Jule Gregory Charney*, Springer, 1948, pp. 251–265.

[23] W. Horton and A. Hasegawa, "Quasi-two-dimensional dynamics of plasmas and fluids," *Chaos: An Interdisciplinary Journal of Nonlinear Science*, vol. 4, no. 2, pp. 227–251, 1994.

[24] J. A. Crotinger and T. H. Dupree, "Trapped structures in drift wave turbulence," *Physics of Fluids B: Plasma Physics*, vol. 4, no. 9, pp. 2854–2870, 1992.

[25] G. Botha, M. Haines, and R. Hastie, "The effect of sheared diamagnetic flow on turbulent structures generated by the charney–hasegawa–mima equation," *Physics of Plasmas*, vol. 6, no. 10, pp. 3838–3852, 1999.

[26] C. Lashmore-Davies, A. Thyagaraja, and D. McCarthy, "Spectral transfers and zonal flow dynamics in the generalized charney-hasegawa-mima model," *Physics of plasmas*, vol. 12, no. 12, 2005.

[27] S. Gallagher, B. Hnat, C. Connaughton, S. Nazarenko, and G. Rowlands, "The modulational instability in the extended hasegawa-mima equation with a finite larmor radius," *Physics of Plasmas*, vol. 19, no. 12, 2012.

[28] N. Sato and M. Yamada, "A generalized hasegawa–mima equation in curved magnetic fields," *Journal of Plasma Physics*, vol. 88, no. 3, p. 905 880 319, 2022.

[29] N. Sato and M. Yamada, "An extended hasegawa–mima equation for nonlinear drift wave turbulence in general magnetic configurations," *Physica D: Nonlinear Phenomena*, vol. 459, p. 134 031, 2024.

[30] S. M. Moufawad and N. R. Nassif, "Newton type methods for solving a hasegawa–mima plasma model," *Applied Mathematics and Computation*, vol. 459, p. 128 141, 2023.

[31] R. Alam, J. Khetia, S. Shin, *et al.*, "Physics of a tokamak,"

[32] D. J. Griffiths, "Introduction to electrodynamics fourth edition," 2021.

[33] M. Cavedon, T. Pütterich, E. Viezzer, *et al.*, "Pedestal and er profile evolution during an edge localized mode cycle at asdex upgrade," *Plasma Physics and Controlled Fusion*, vol. 59, no. 10, p. 105 007, 2017.

[34] M. Murakami, M. Wade, J. DeBoo, *et al.*, "Advanced tokamak profile evolution in diii-d," *Physics of Plasmas*, vol. 10, no. 5, pp. 1691–1697, 2003.

[35] M. Kočan, J. Gunn, S. Carpentier-Chouchana, *et al.*, "Measurements of ion energies in the tokamak plasma boundary," *Journal of Nuclear Materials*, vol. 415, no. 1, S1133–S1138, 2011.

[36] J. W. Bush, "Surface tension module," *URL http://web. mit. edu/1.63/www/Lecnotes/Surfacetension*, 2004.

[37] F. Hecht, "New development in freefem++," *Journal of numerical mathematics*, vol. 20, no. 3-4, pp. 251–266, 2012.

[38] P. D. Foote, *" Center of Gravity" and" effective Wave Length" of Transmission of Pyrometer Color Screens, and the Extrapolation of the High Temperature Scale*. US Government Printing Office, 1916, vol. 12.

[39] A. Hasegawa and M. Wakatani, "Plasma edge turbulence," *Physical Review Letters*, vol. 50, no. 9, p. 682, 1983.

[40] I. Goumiri, C. W. Rowley, Z. Ma, D. Gates, J. Krommes, and J. Parker, "Reduced-order model based feedback control of the modified hasegawa-wakatani model," *Physics of Plasmas*, vol. 20, no. 4, 2013.

[41] T. Stoltzfus-Dueck, B. Scott, and J. Krommes, "Nonadiabatic electron response in the hasegawa-wakatani equations," *Physics of Plasmas*, vol. 20, no. 8, 2013.

[42] S. Kondo, "Almost-periodic solution of linearized hasegawa–wakatani equations with vanishing resistivity," *Rendiconti del Seminario Matematico della Università di Padova*, vol. 133, pp. 215–240, 2015.

[43] S. Kondo, "Global-in-time existence results for the two-dimensional hasegawa–wakatani equations," *Annali di Matematica Pura ed Applicata (1923-)*, vol. 197, no. 6, pp. 1799–1819, 2018.

[44] R. Numata, R. Ball, and R. L. Dewar, "Bifurcation in electrostatic resistive drift wave turbulence," *Physics of Plasmas*, vol. 14, no. 10, 2007.

[45] D. Del Sarto and A. Ghizzo, "Hasegawa–wakatani and modified hasegawa–wakatani turbulence induced by ion-temperature-gradient instabilities," *Fluids*, vol. 2, no. 4, p. 65, 2017.

[46] R. Hajjar, *Ecology of Flows and Drift Wave Turbulence: Reduced Models and Applications*. University of California, San Diego, 2018.

[47] C. Gahr, I.-G. Farcas, and F. Jenko, "Learning physics-based reduced models from data for the hasegawa-wakatani equations," *arXiv preprint arXiv:2401.05972*, 2024.

[48] J. Dewhurst, B. Hnat, and R. Dendy, "The effects of nonuniform magnetic field strength on density flux and test particle transport in drift wave turbulence," *Physics of Plasmas*, vol. 16, no. 7, 2009.

[49] S. B. Korsholm, *Coherent structures and transport in drift wave plasma turbulence*. Risø National Laboratory, 2002.